

~~SECRET~~

NAA-SR-286



n.o. 42923

**RADIATION EFFECTS
QUARTERLY PROGRESS REPORT
JULY—SEPTEMBER, 1953**

**EDITED BY:
F. E. FARIS**

Photostat Price \$ 7.80
Microfilm Price \$ 3.30
Available from the
Office of Technical Services
Department of Commerce
Washington 25, D. C.

**ATOMIC ENERGY RESEARCH DEPARTMENT
NORTH AMERICAN AVIATION, INC.
P. O. BOX 309 DOWNEY, CALIFORNIA**

SUBMITTED: NOVEMBER 12, 1953

**ISSUE DATE
APRIL 15, 1954**

1246 001

CONTRACT AT 11-1-GEN-8

1 5794

SECRET
1246



TABLE OF CONTENTS

	Page No.
I. Graphite	7
A. Thermal Conductivity.	7
B. Magnetic Susceptibility	14
C. Cyclotron Irradiations of Graphite	17
D. Annealing Kinetics.	24
E. Asymptotic Aging Experiments	26
II. Metals	33
A. Effects of Impurities on the Recovery of Electrical Resistivity in Cold-Worked Copper	33
B. Measurements of Thermoelectric Power and Electrical Resistivity of Copper	36
C. Elastic Constants and Internal Friction.	37
D. Radiation Effects in Metastable Alloys	38
III. Insulators	40
A. Mechanical Effects of Ionizing Radiation in Insulators .	40
B. Optical Effects in Alkali Halides	41
IV. Cyclotron Operation and Development	45
A. Operation	45
B. Radiation Effects on Thermoelectric Power of Iron. .	45
C. Rotating Target Holder	46
D. Mass Transfer	46
E. Physical Length Change of Graphite	46
V. Reactor Irradiation	49
A. Capsule Exposure	49
B. In-Pile and Related Experiments	49
References	50



LIST OF FIGURES

	Page No.
1. Thermal Conductivity of Various Graphite Types	10
2. Thermal Conductivity of Type AGOT-KC (Longitudinal) Graphite	11
3. Thermal Conductivity of Type AWG (Parallel) Graphite	11
4. Thermal Resistivity Change Caused by Neutron Irradiation as a Function of Temperature	12
5. Thermal Resistivity Change Caused by Neutron Irradiation as a Function of Exposure	12
6. Electrical Resistivity of Type AGOT-KC (Longitudinal) Graphite	13
7. Electrical Resistivity of Type AWG (Parallel) Graphite	13
8. Effect of Neutron Bombardment on Magnetic Properties of Graphite	15
9. Effect of Annealing on Magnetic Properties of Irradiated (460 mwd/ct) Graphite	16
10. Effect of Annealing on Magnetic Properties of Irradiated (1534 mwd/ct) Graphite	16
11. Arrangement of Graphite Target for In-Place Measurements of Thermoelectric Power and Electrical Resistivity	19
12. Electrical Resistivity of Irradiated and Unirradiated Graphite as a Function of Temperature	19
13. Thermoelectric Power of Irradiated and Unirradiated Graphite as a Function of Temperature	20
14. Electrical Resistivity of Graphite as a Function of Exposure for Various Temperatures	20
15. Thermoelectric Power of Graphite at 293° K as a Function of Exposure	21
16. Thermoelectric Power of Graphite at 150° K as a Function of Exposure	21
17. Thermoelectric Power of Parallel-Cut AWG Graphite after Pulse Annealing at Various Temperatures	22
18. Electrical Resistivity of Parallel-Cut AWG Graphite after Pulse Annealing at Various Temperatures	22



LIST OF FIGURES (Continued)

	Page No.
19. Thermoelectric Power of Parallel-Cut AWG Graphite as a Function of Temperature. (Specimen No. 1)	23
20. Thermoelectric Power of Parallel-Cut AWG Graphite as a Function of Temperature. (Specimen No. 2)	23
21. Electrical Resistivity at 40° C <u>vs</u> Time of Various Successive Annealing Temperatures	25
22. Stored Energy Release from Irradiated Graphite Annealed in an Oven at 183° C	30
23. Thermal Annealing of 12.5 md/ct Irradiated Graphite	30
24. Tempering Curves Showing Recovery of Residual Electrical Resistivity of Cold-Worked Pure Copper and Copper Containing Silver and Zinc Impurities	35
25. Optical Absorption of Additively Colored KCl after 180 hours at 150° C (Annealed in Dark)	43
26. Optical Absorption of Additively Colored KCl after 50 minutes at 150° C (Annealed in Daylight)	44
27. Optical Absorption of Additively Colored KCl after 180 hours at 150° C (Annealed in Daylight)	44
28. Thermoelectric Power <u>vs</u> Temperature for Iron-Irradiated Iron	48



I. GRAPHITE

A. Thermal Conductivity (A. W. Smith, J. E. Hove, N. S. Rasor)

The study of the thermal conductivity of graphite is a part of the complete study of the physical properties of graphite. Early results showed this property to be one of lattice conduction rather than electron conduction. Thermal conductivity is dependent on crystallite size as well as lattice imperfections; and for this reason, the different types of artificial graphite show a correlation between the crystallite size and the thermal conductivity. Figure 1 shows the conductivity of the various types of graphite. The larger the crystallite size of the graphite (as determined by X-ray measurements), the higher is the conductivity. Due to uncertain orientation and density corrections as well as the anomalous temperature dependence of the thermal conductivity, a quantitative relationship between thermal conductivity and particle size cannot be derived.

The effect of increasing lattice imperfections by neutron bombardment is to decrease the conductivity. In this study, the temperature dependence as well as the absolute magnitude of the conductivity is important. The dimensions and the nature of the scattering centers will affect the temperature dependence of the conductivity. It should be noted that the temperature dependence of unirradiated graphite, both in the artificial and natural polycrystalline states, is anomalous. The limiting slope of a log conductivity versus log temperature plot (i. e., the power of the temperature dependence) should not be greater than that of the heat capacity. Any kind of scattering should decrease the slope. However, graphite shows a limiting slope of nearly three for the thermal conductivity while the corresponding slope for the heat capacity does not become greater than two in the same temperature range. Although much time has been spent exploring the basic theory of heat conductivity and applying it to graphite, no completely adequate explanation has been found. While this problem is still being investigated, the study of the effect of radiation damage is also being carried forward.

Figures 2 and 3 show the effect of neutron bombardment on types AGOT-KC and AWG graphite. Data on type SA-25 have been previously reported.¹ Assuming that the thermal resistivities due to different scattering mechanisms



may be treated as approximately additive, the increased resistivity resulting from exposure may be separated and examined. This resistivity increase is shown in Figs. 4 and 5.

It may be noted from Fig. 4 that for low temperatures, the increase in the resistivity has a dependence on temperature varying, for the AGOT-KC, from $T^{-1.8}$ at low exposures (e. g., 12.5 mwd/ct) to about $T^{-1.5}$ at higher exposures. Although there is some uncertainty for the sample irradiated for 1927 mwd/ct, the negative temperature exponent may be represented quite closely by $2 - \log(1 + t)^{0.17}$, where t is the exposure time in mwd/ct. This indicates that, for low temperature and low damage, the thermal resistance caused by neutron bombardment varies as T^{-2} .

From Fig. 5 it can be seen that for low damage the incremental thermal resistance also varies as a fractional power of t , the exposure time. For low temperature the slope appears to approach $2/3$ and the value $(2/3 + 0.9 \times 10^{-3} t + 0.0235 \sqrt{t})$ will also fit the data within the estimated error. It is tempting to accept this latter expression, since a preliminary treatment of the scattering of phonons by electrons in graphite² indicates that the thermal resistance due to this mechanism will vary as $t^{1/2}$. The possibility of electron scattering was originally suggested by J. Krumhansl.³ The rather crude treatment attempted thus far gives an incremental thermal resistivity varying either as T^{-1} or T^{-2} depending on the assumptions made. This uncertainty is connected with the anomalous temperature dependence of the thermal conductivity of unirradiated graphite. Further work to clarify this point is in progress.

Data for Types AWG and SA-25 graphite are also shown in Figs. 4 and 5. Although there is a considerable scatter in the SA-25 results, the values are in qualitative agreement with those for Type AGOT-KC. Although there are only meager data for Type AWG (two irradiation times), a good quantitative agreement with AGOT-KC is found.

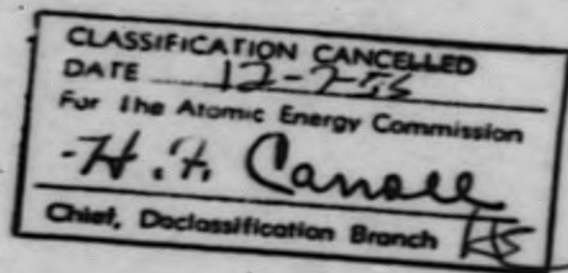
While more detailed calculations are being made on the effect of scattering by electrons, an experimental investigation using brom-graphite compounds is also being started to elucidate the effect of electrons on the thermal conductivity of graphite. A further study employing alkali halides containing colloidal



particles has also been started in order to determine experimentally the role of different kinds of imperfections in scattering phonons.

Thermal diffusivity, being proportional to the thermal conductivity divided by the specific heat, is theoretically proportional to the product of the group velocity and the mean free path of the phonons. Measurements have been made of the diffusivity of damaged AGOT and of index rod. These measurements have given a value of the diffusivity that is lower than calculated. However, since this is a transient measurement, the contact between the temperature measuring probe and the sample is extremely critical. In fact it has been shown that the apparent diffusivity will change upon changing the mass and the degree of contact of the probe. For this reason these measurements are not reported here.

The electrical resistivity of each sample was measured simultaneously with the thermal conductivity. The results for Type AGOT-KC and Type AWG graphite are shown in Figs. 6 and 7. Due to the small size of the samples and the number of flaws and strains, the absolute value of each measurement is subject to an error of the order of 10 per cent for the better samples and more than this for the damaged ones.



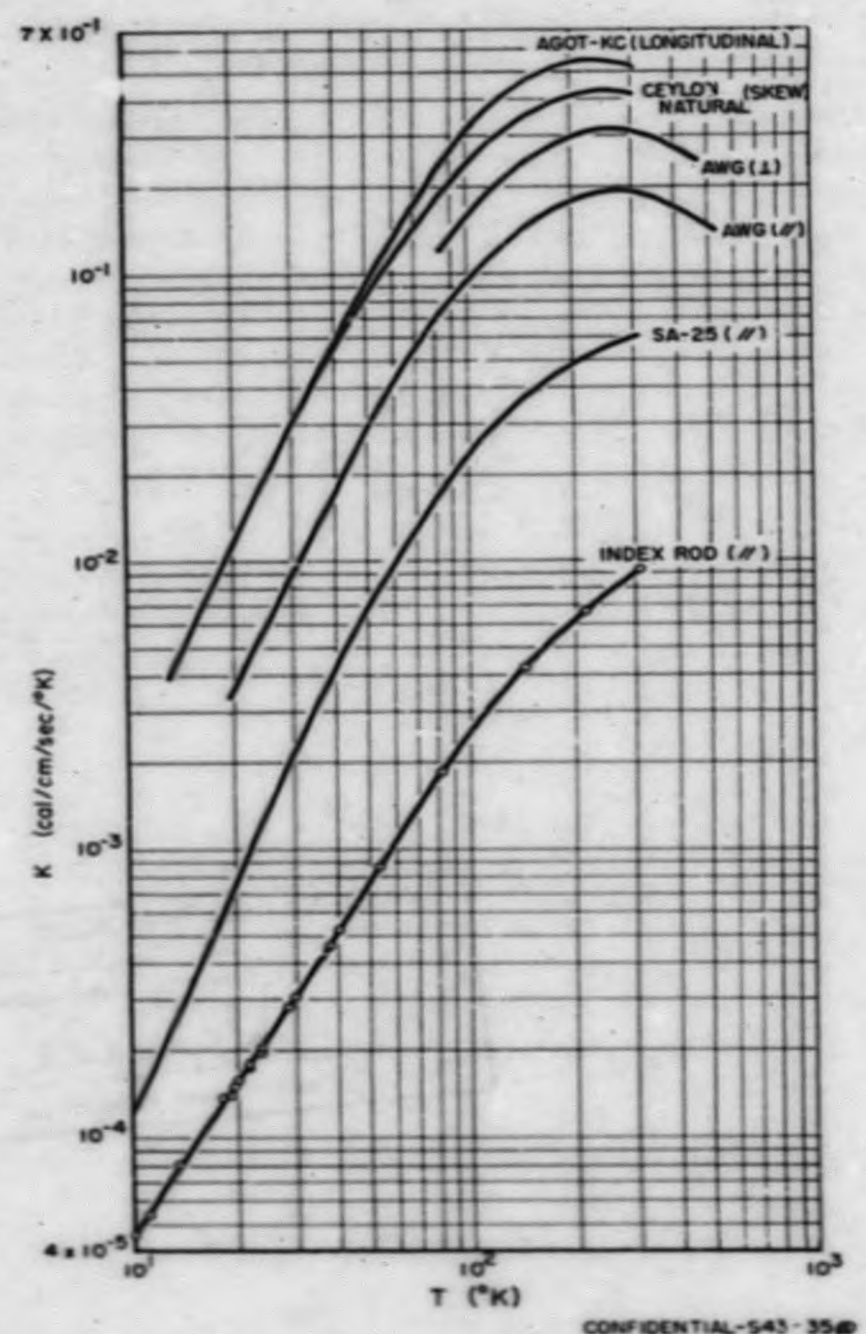


Fig. 1. Thermal Conductivity of Various Graphite Types

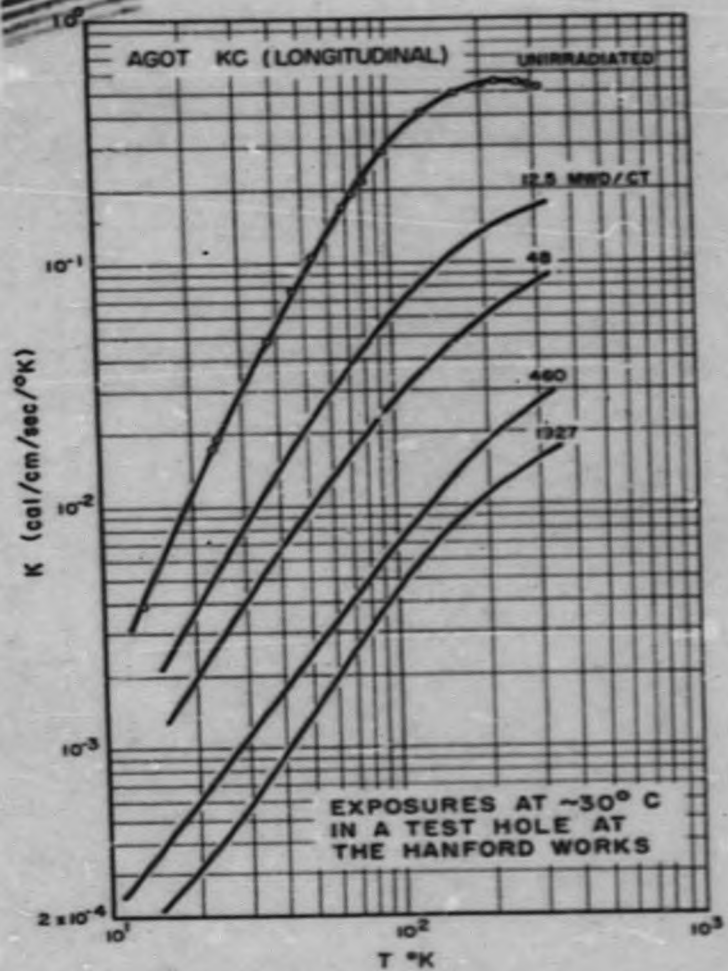


Fig. 2. Thermal Conductivity of Type AGOT-KC (Longitudinal) Graphite

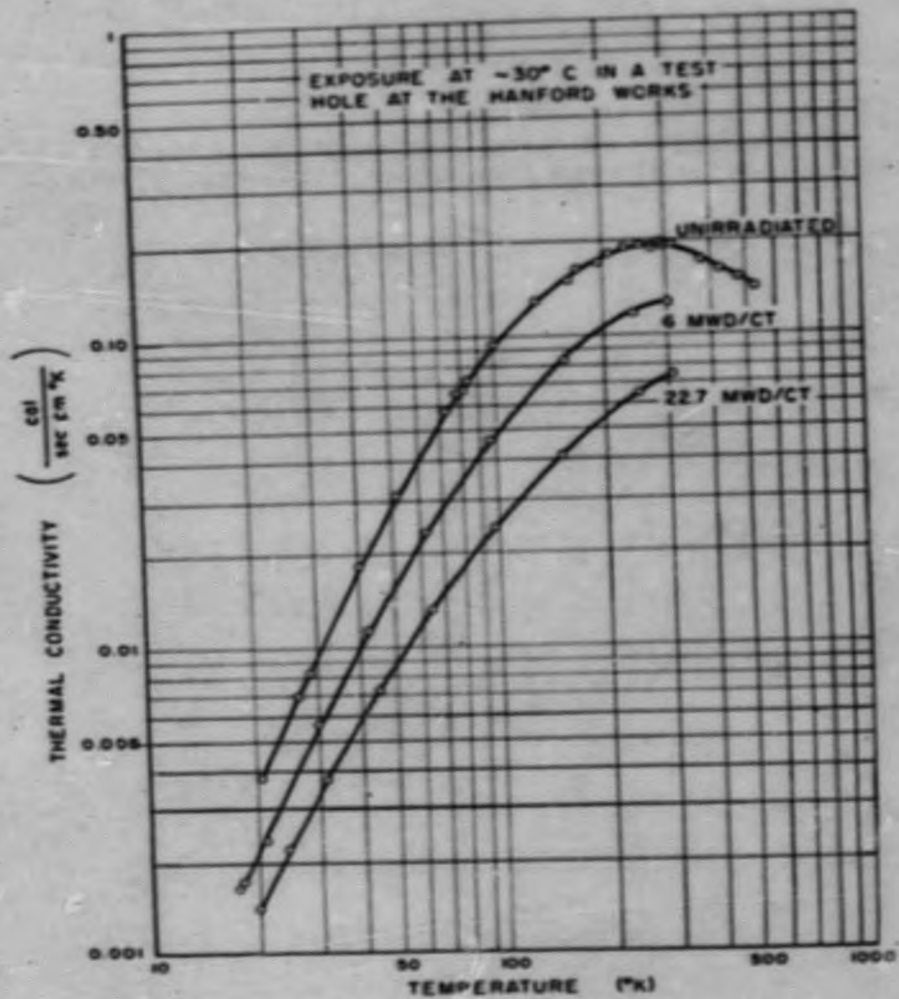


Fig. 3. Thermal Conductivity of Type AWG (Parallel) Graphite

1246 009

11

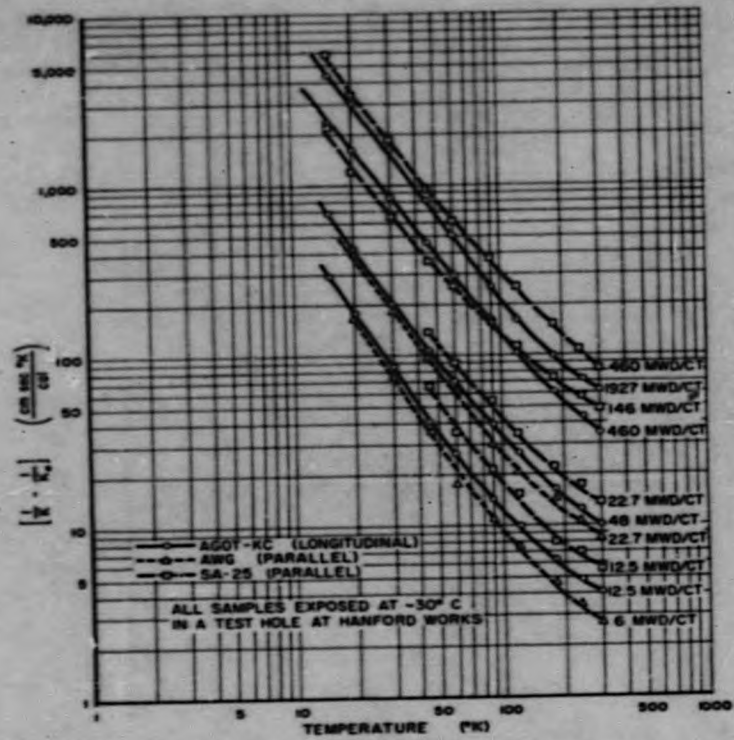


Fig. 4. Thermal Resistivity Change Caused by Neutron Irradiation as a Function of Exposure

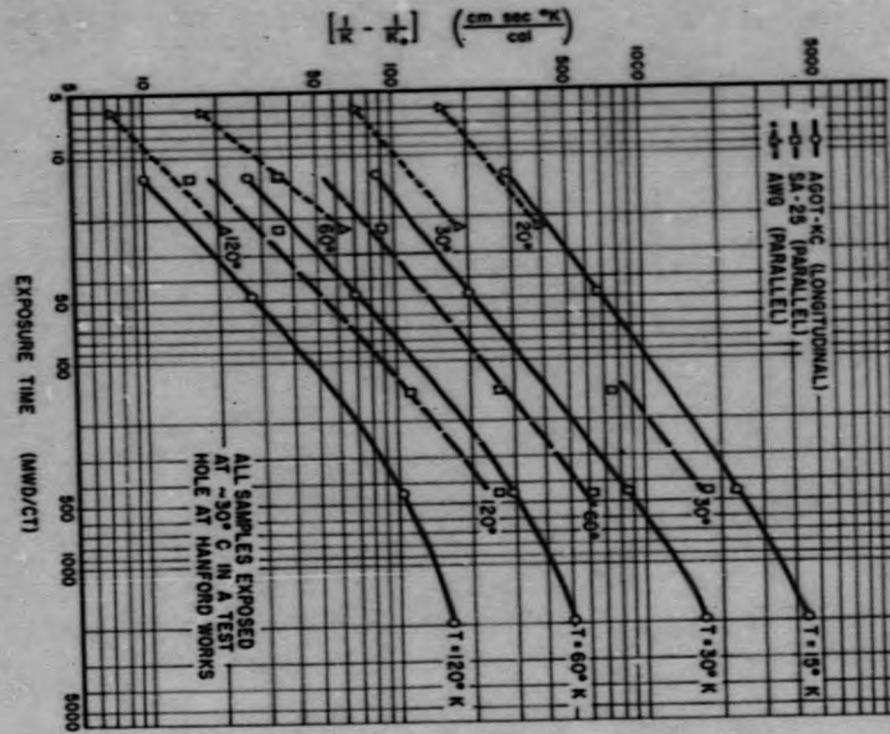


Fig. 5. Thermal Resistivity Change Caused by Neutron Irradiation as a Function of Exposure

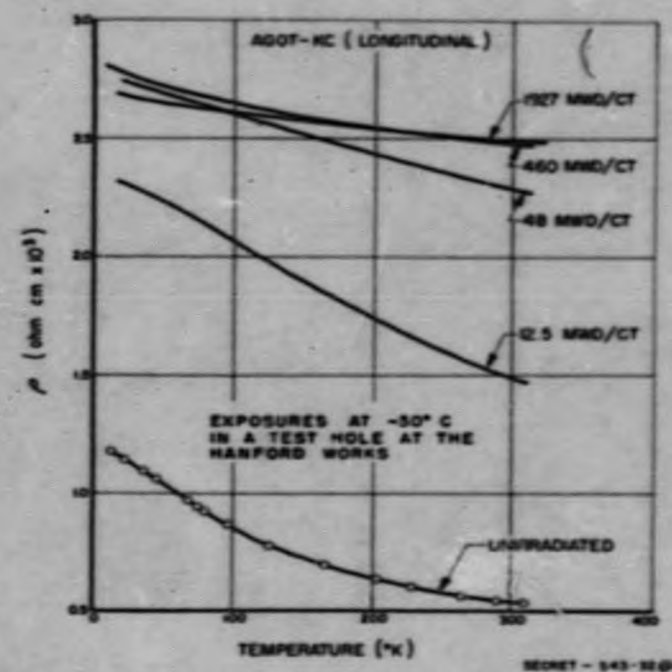


Fig. 6. Electrical Resistivity of Type AGOT-KC (Longitudinal) Graphite

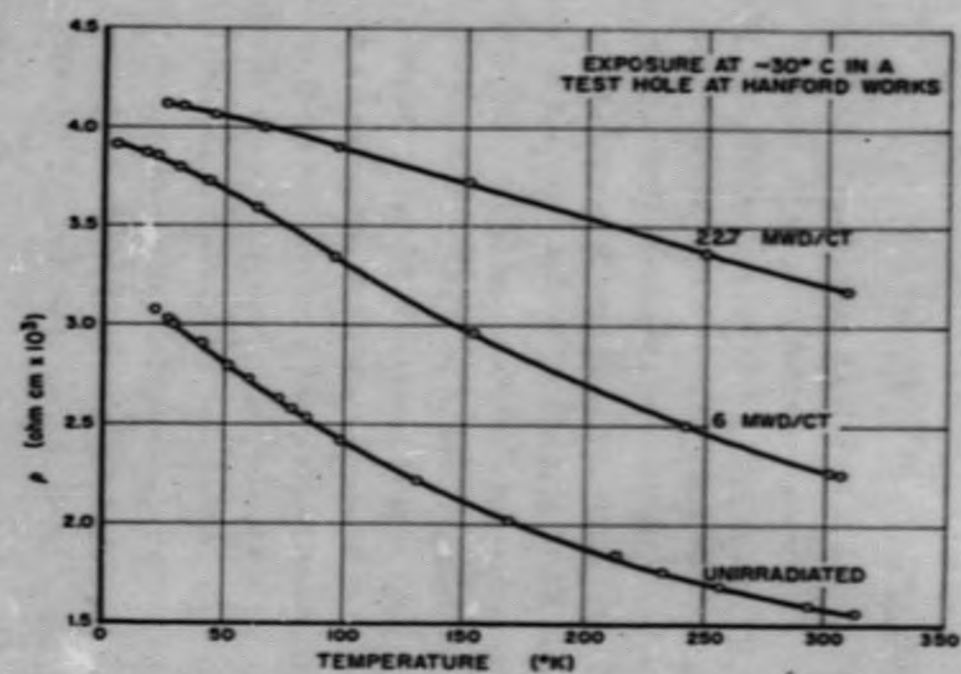


Fig. 7. Electrical Resistivity of Type AWG (Parallel) Graphite

1246 011

13

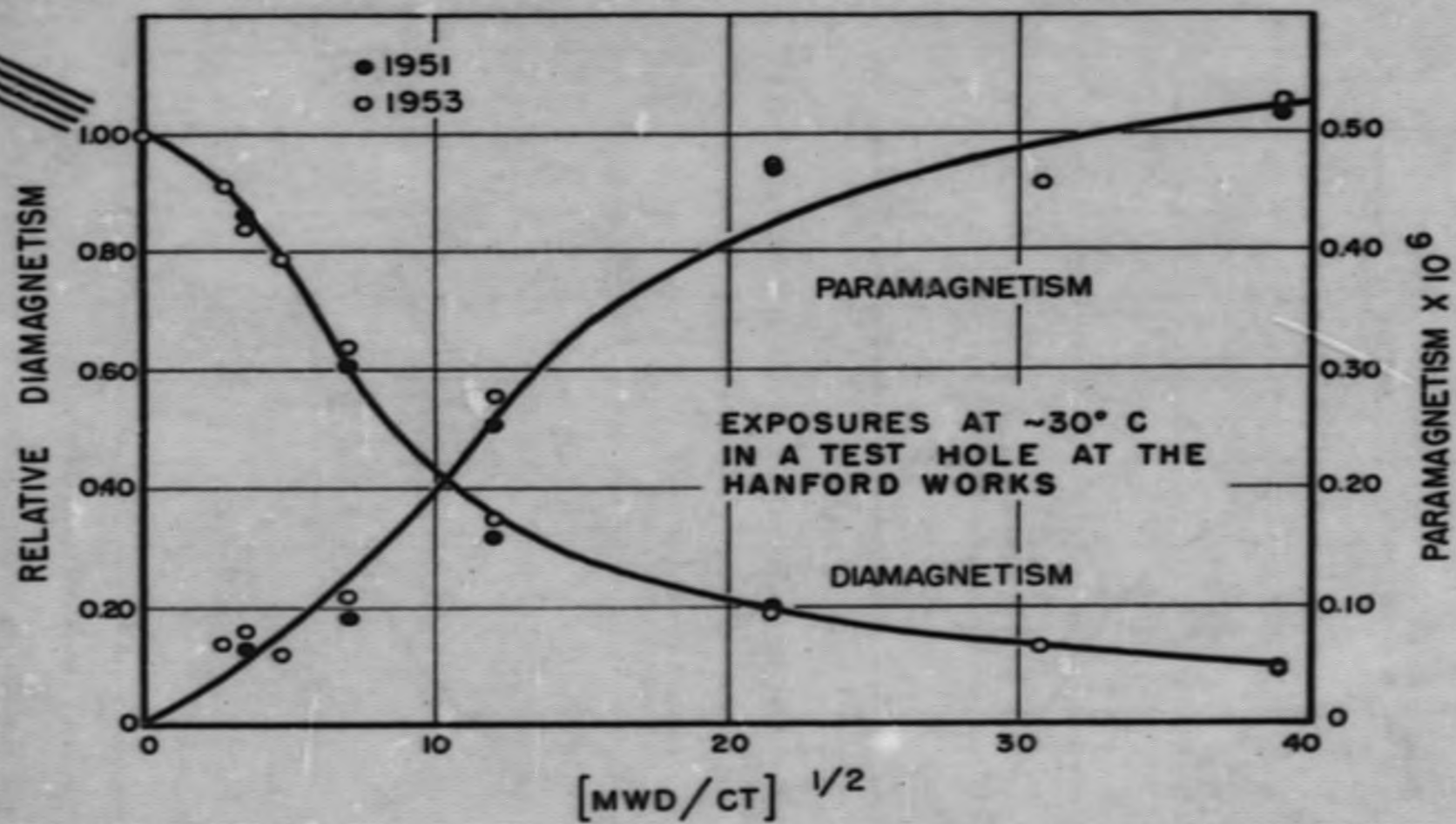
SECRET

▲

B. Magnetic Susceptibility (J. D. McClelland)

It was pointed out in the last progress report⁴ that it is possible to separate out the Peierls diamagnetism from the paramagnetism by noting the changes in the anisotropy ratio. This separation requires, however, accurate determinations of the magnetic susceptibility, the usual precision leading to rather large errors in the determination of the paramagnetic term. Therefore, measurements with greater precision have been made on a second set of samples with irradiations of 7.6, 12.5, 22.7, 48, 146, 460, and 1534 mwd/ct. The susceptibility of each sample was measured in three orthogonal directions before and after annealing at 2000° C for a period of 10 minutes. Previous evidence indicates that complete recovery to the pre-irradiation value occurs at this temperature. Following the procedure outlined in the preceding progress report,⁴ the fractional decrease in the Peierls diamagnetism as well as the increase in the paramagnetism as a result of neutron bombardment was obtained. Figure 8 shows the results of such an analysis compared with the results reported previously. Close agreement exists between the two sets of data. Annealing data for graphite with exposures of 460 mwd/ct and 1534 mwd/ct have also been analyzed. The results are shown in Figs. 9 and 10.

The experimental error present in the paramagnetic term is about $\pm 0.04 \times 10^{-6}$ emu while that in the fractional decrease of the Peierls terms is $\pm 3/4$ per cent. The effect of separating out the paramagnetic term is to smooth out the curves, especially in the region from 200 to 500° C. Curves for the un-separated susceptibility show a sudden break at the onset of annealing. It now appears that this is due to a sudden decrease in the paramagnetism rather than to a change in the Peierls term. It is interesting to note that in the region from 500 to 1400° C, where the Peierls diamagnetism is increasing rapidly, the paramagnetism seems to remain constant. In the region beyond 1400° C where only small changes occur in the Peierls term, a sudden decrease once again appears in the paramagnetism.



1246 0135

S43-30@
SECRET

Fig. 8. Effect of Neutron Bombardment on Magnetic Properties of Graphite

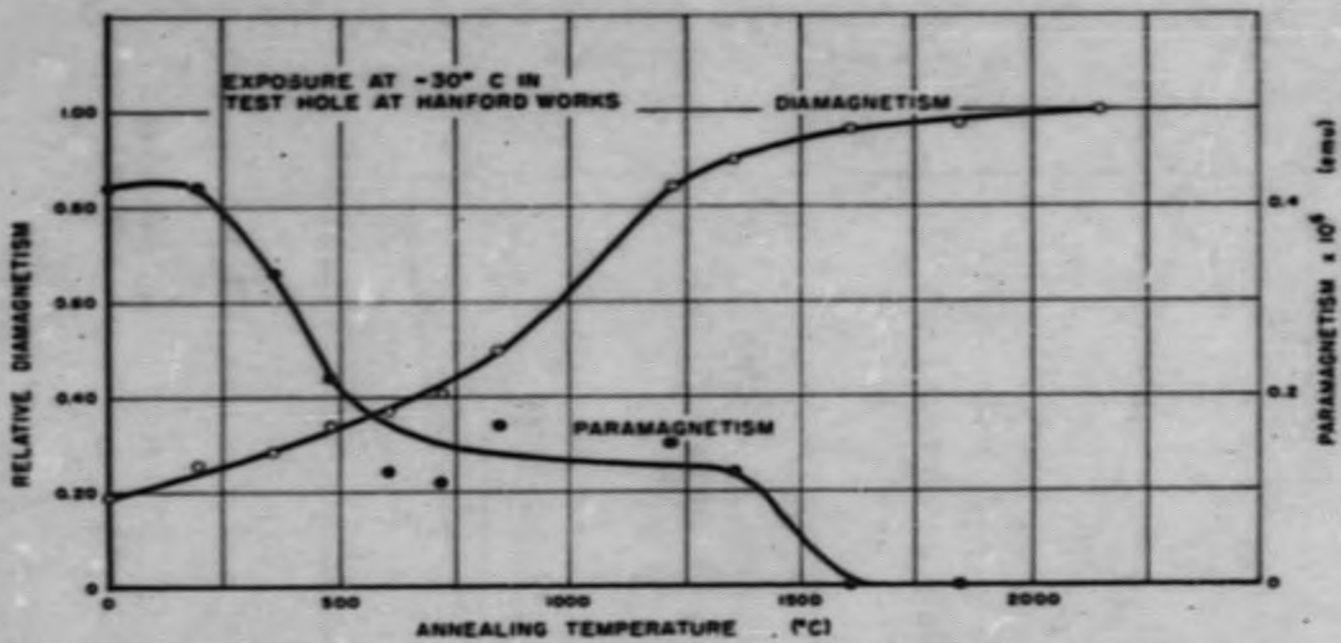


Fig. 9. Effect of Annealing on Magnetic Properties of Irradiated (460 mwd/ct) Graphite

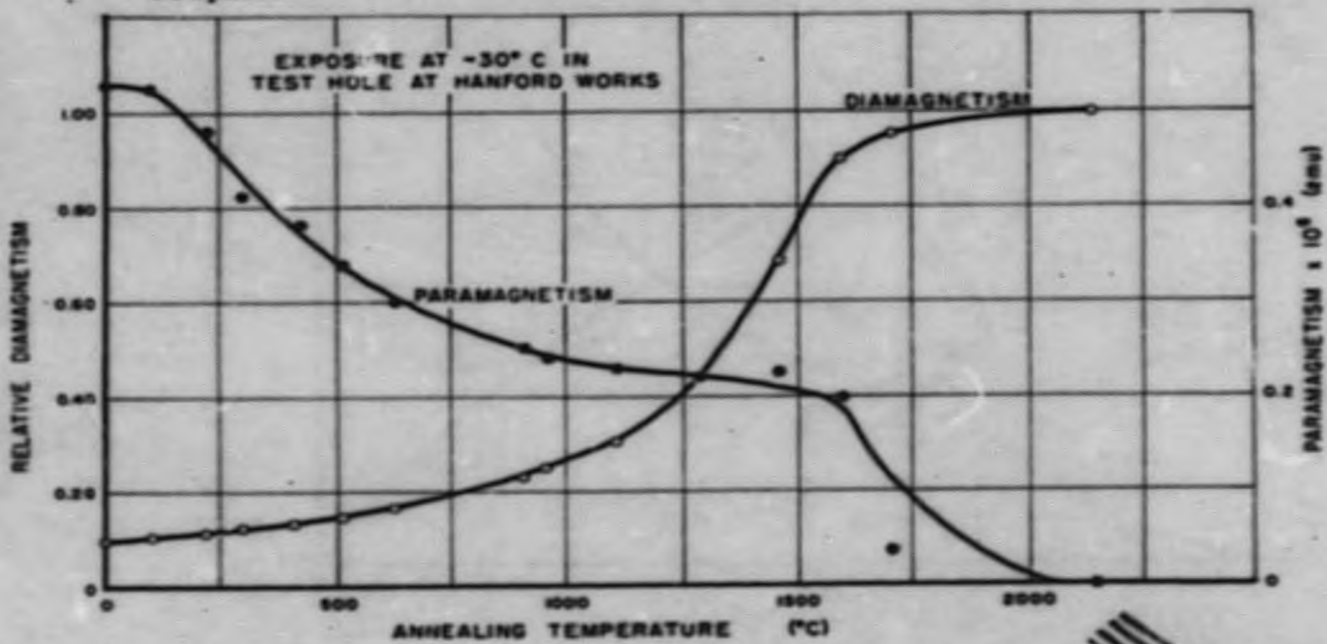


Fig. 10. Effect of Annealing on Magnetic Properties of Irradiated (1524 mwd/ct) Graphite

C. Cyclotron Irradiations of Graphite

1. In-Place Measurements (W. S. Gilbert, D. L. Clark) Type AWG graphite was irradiated with 10-Mev protons at + 30° C with in-place determinations of electrical resistivity, ρ , and thermoelectric power, Q , being made periodically. The measurements were made at various temperatures from -190 to 20° C at exposures up to $12 \mu\text{ah}/\text{cm}^2$. Figure 11 is a photograph of the target with 3-mil copper-constantan thermocouples attached.

Pile irradiated AWG graphite has been investigated by Eatherly and Rasor,⁵ so that one is able to compare the damaging effects of neutrons and charged particles. The two sets of data are not exactly comparable since the cyclotron data was obtained immediately after the specified irradiation; whereas the pile-irradiated graphite was not measured for approximately one year after the irradiation and was kept at room temperature during this interval. Appreciable annealing was observed during a 14-day period at room temperature in the case of the cyclotron samples. Figures 12 and 13 are graphs of ρ and Q vs T for various amounts of both pile and cyclotron irradiation. From Figs. 12 and 13, it can be seen that the pile and cyclotron modes of damage accumulation are more similar for ρ than for Q . The deviations are more pronounced toward lower temperatures.

If one plots ρ vs exposure and uses as a correlation factor $1.0 \mu\text{ah}/\text{cm}^2$ protons = 1.5 mwd/ct in a Hanford pile, one obtains Fig. 14. Using the same factor, one obtains Q vs exposure for $T = 293^\circ \text{K}$ as shown in Fig. 15. The correlation is not so good for Q at the lower temperatures, as is apparent from Fig. 16.

The direct effects of pile irradiation and cyclotron irradiation on graphite have not been compared because the differences in the annealing for the samples studied were not taken into account. At the present time ρ has been measured to ± 0.1 per cent and Q to $+ 1.0 \mu\text{v}/^\circ\text{K}$ with the sample in-place on the cyclotron. Modifications are in progress to increase the precision and the speed of measurement and to extend the temperature range to above + 300° C. By making irradiations at different temperatures and by long-term annealing studies, we hope to be able to separate the damaging and annealing processes.



2. Annealing Experiments (G. E. Deegan) - The annealing of specimens which were preserved at a low temperature subsequent to cyclotron alpha-particle irradiation at -180°C has been previously described.⁶ This work has been continued. Two additional 4-mil-thick layers of the laminated set E-1 of cyclotron run 522B ($2.6\ \mu\text{ahr}/\text{cm}^2$) have been examined for changes in the thermoelectric power, Q , and the electrical resistivity, ρ . Figures 17 and 18 show the changes in Q and ρ as a function of pulse annealing temperature for the layers measured. The results for layers 1 and 2 confirm the initial decrease in Q and the increase in ρ previously reported for layer No. 5⁶ and shown again for convenience in the figures.

The resistivity vs pulse-temperature curves (Fig. 18) are useful only in indicating the annealing rates, as the absolute values are undoubtedly in error. Resistivity-range experiments⁷ indicate that the resistance should increase with depth. Layer No. 5, for which the average distance traveled by the particles in graphite was 18 mils, should have a value of resistivity larger by a factor of 2 than layer No. 1 (average distance traveled by particles = 2 mils).

The most interesting feature of these measurements, aside from the existence of the low temperature annealing state, is the departure of the temperature dependence of the thermoelectric power, shown in Figs. 19 and 20, from that observed for pile irradiated graphite.⁵ Since this difference is also found for graphite bombarded at room temperature on the cyclotron (cf. preceding section), it apparently is not a phenomenon associated with the temperature of irradiation but is rather an intrinsic damage or annealing effect.

New apparatus is under construction in order to provide a device for the measurement of the temperature dependence of the thermoelectric power, the electrical resistivity, and the thermal conductivity down to 4°K during the pulse annealing runs. It is also planned to carry out low temperature isothermal anneals in order to learn more about the behavior of the low-temperature state. More samples of parallel-cut AWG irradiated at Hanford are now on hand, and these will be examined in order to fill in earlier data⁵ and extend it to higher exposures.



Fig. 11. Arrangement of Graphite Target for In-Place Measurements of Thermoelectric Power and Electrical Resistivity

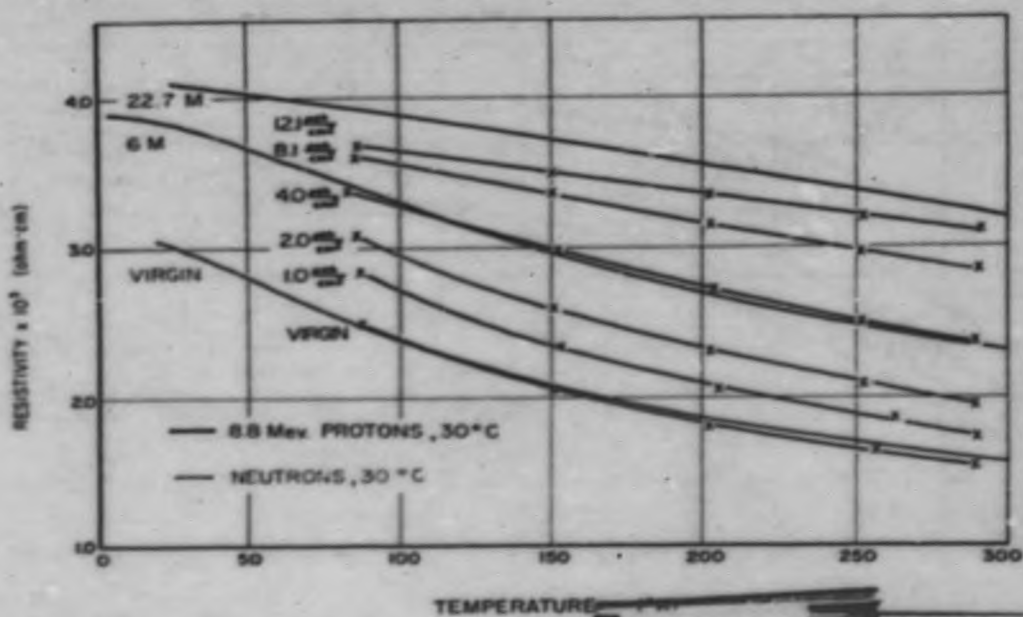


Fig. 12. Electrical Resistivity of Irradiated and Unirradiated Graphite as a Function of Temperature

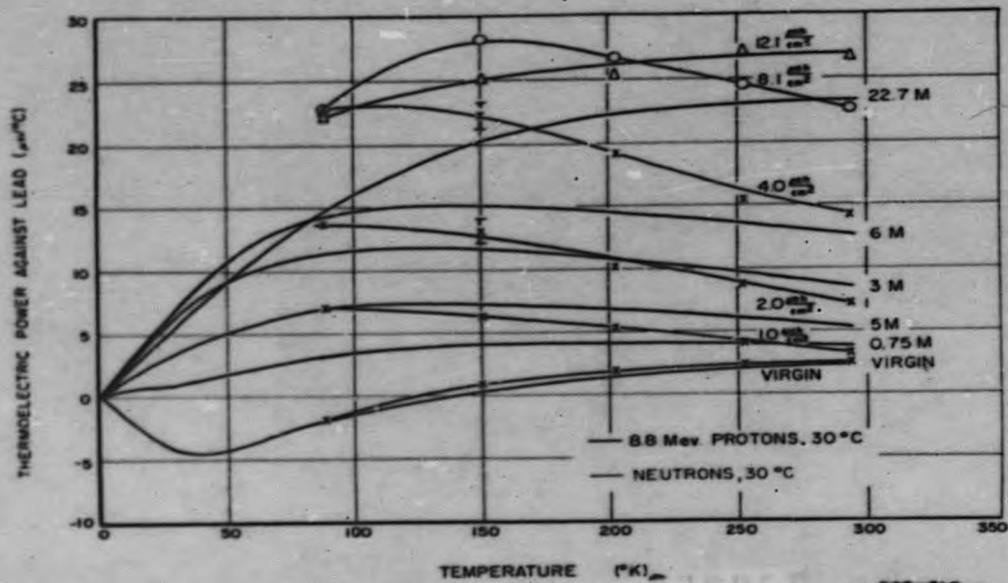


Fig. 13. Thermoelectric Power of Irradiated and Unirradiated Graphite as a Function of Temperature

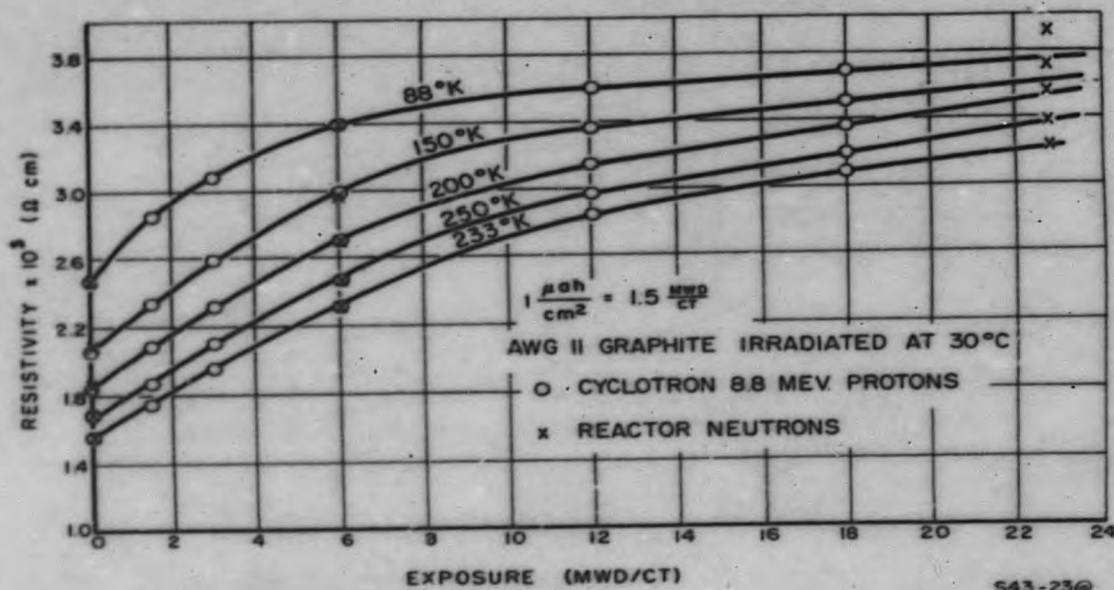


Fig. 14. Electrical Resistivity of Graphite as a Function of Exposure for Various Temperatures

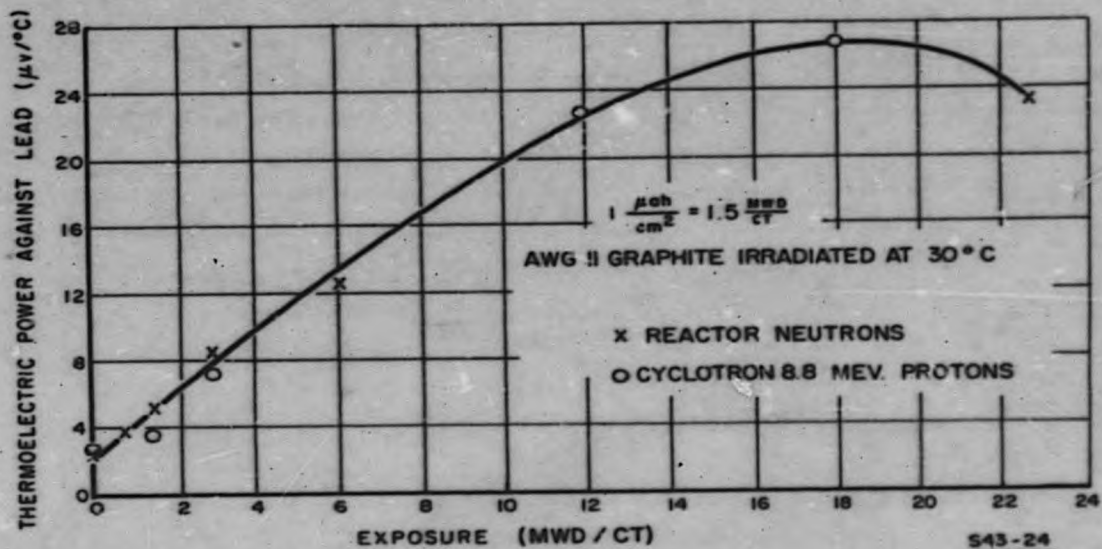


Fig. 15. Thermoelectric Power of Graphite at 293° K as a Function of Exposure

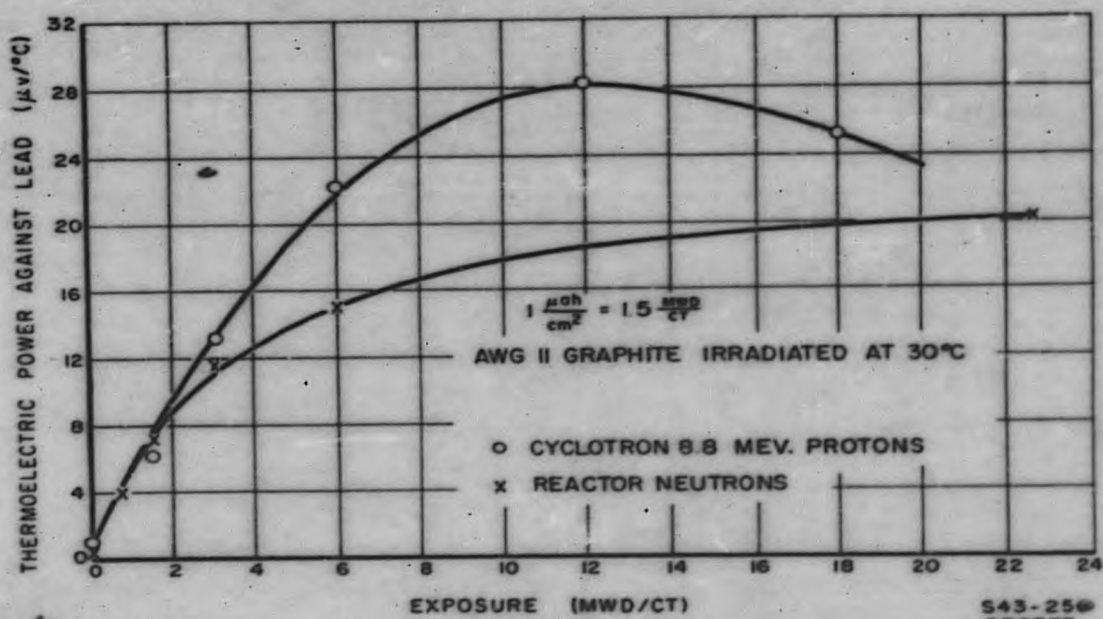


Fig. 16. Thermoelectric Power of Graphite at 150° K as a Function of Exposure

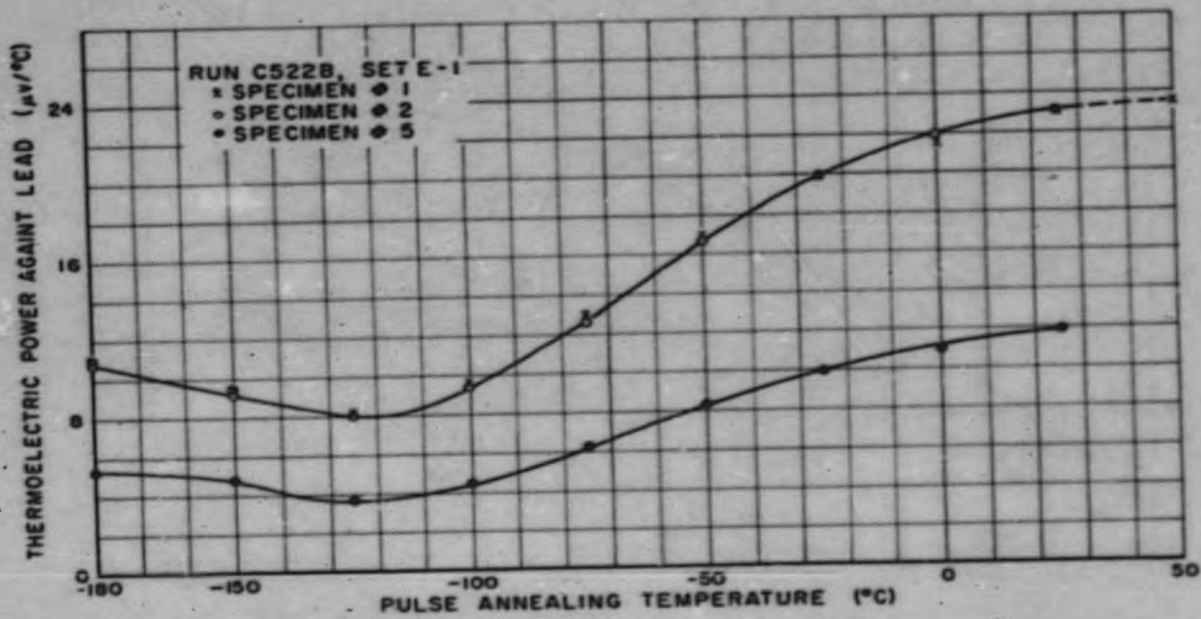


Fig. 17. Thermoelectric Power of Parallel-Cut AWG Graphite after Pulse Annealing at Various Temperatures

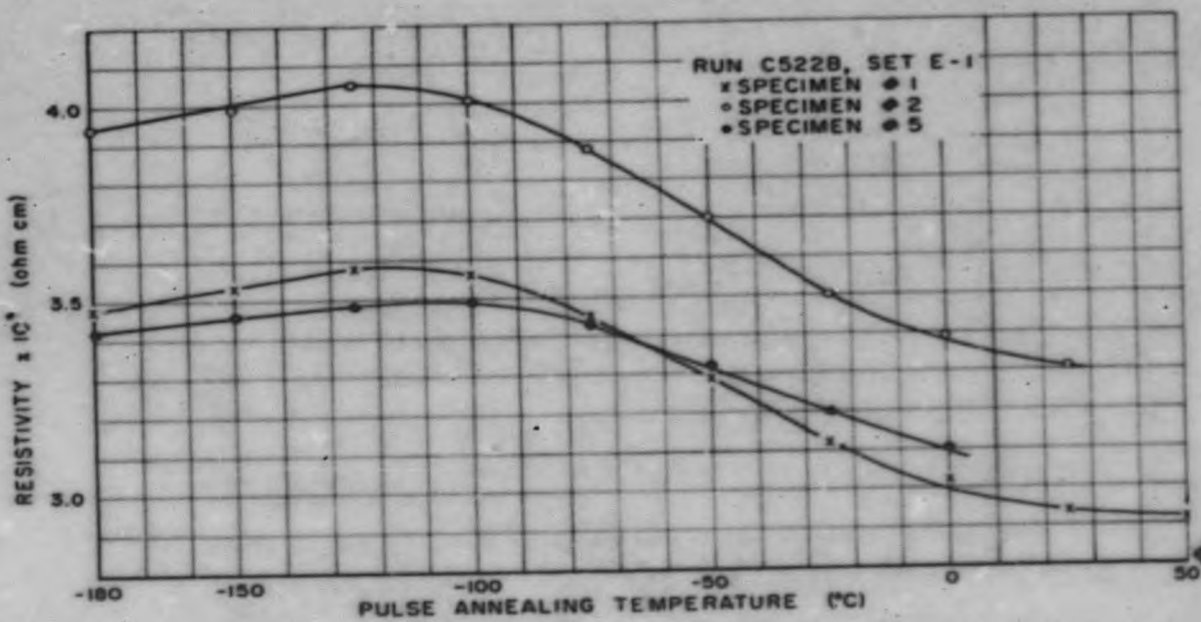


Fig. 18. Electrical Resistivity of Parallel-Cut AWG Graphite after Pulse Annealing at Various Temperatures

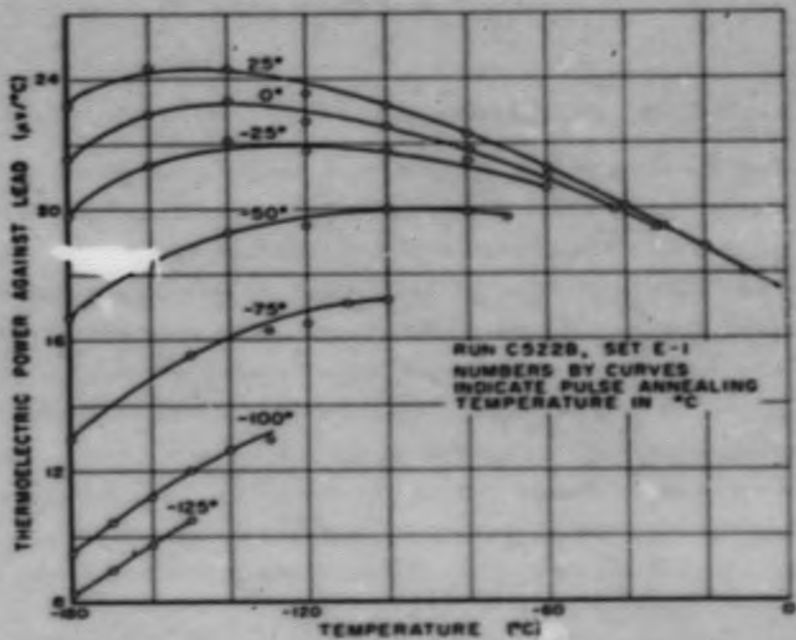


Fig. 19. Thermoelectric Power of Parallel-Cut AWG Graphite as a Function of Temperature (Specimen No. 1)

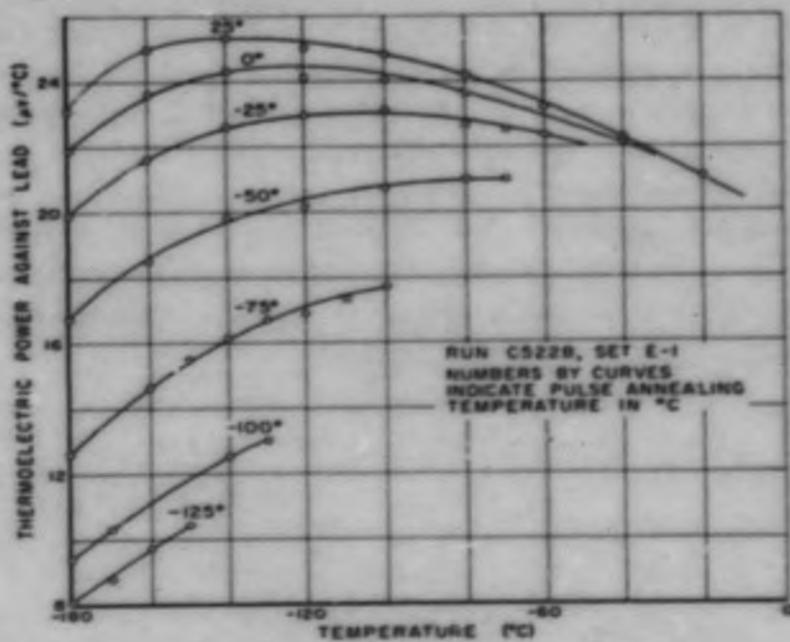


Fig. 20. Thermoelectric Power of Parallel-Cut AWG Graphite as a Function of Temperature (Specimen No. 2)

▲

D. Annealing Kinetics (S. B. Austerman)

Annealing of pile-irradiated graphite is being continued in order to study the annealing characteristics and determine, if possible, the mechanisms by which annealing proceeds. The annealing of two specimens of 48 mwd/ct AGOT-KC graphite from the Hanford Pile is described in previous quarterly progress reports.⁸⁻¹⁰ During the report period, isothermal annealing of a third specimen of the same graphite has been completed; and computations involving the new set of data for electrical and thermal resistivities, and thermoelectric power have also been completed. The computed data are now being analyzed. These data indicates the annealing spectrum to be complex, as though a number of annealing mechanisms may be proceeding simultaneously. That this occurs in at least part of the annealing spectrum is shown by the following preliminary analysis of part of the recent data.

In the annealing region from 1100 to 1250° C the annealing rate of the electrical resistivity behaved erratically as shown in Fig. 21. It is to be seen that for a period of time, an increase of temperature to 1150° C and later to 1200° C caused a reversal in the direction of annealing. This behavior is consistent with, and is suggested by, the annealing data for the two previous specimens studied in this series of experiments and the data presented by Hook.¹¹ Since an equation of the form $\frac{d\rho}{dt} = f(\rho) e^{-E/kT}$ for a single process cannot account for the observed reversal of annealing rate, an annealing involving two processes suggests itself. It was found empirically that the observed rates could be expressed (but not uniquely so) by two annealing processes whose activation temperatures are very roughly 50,000 and 70,000° K and which have opposite effects upon the electrical resistivity.

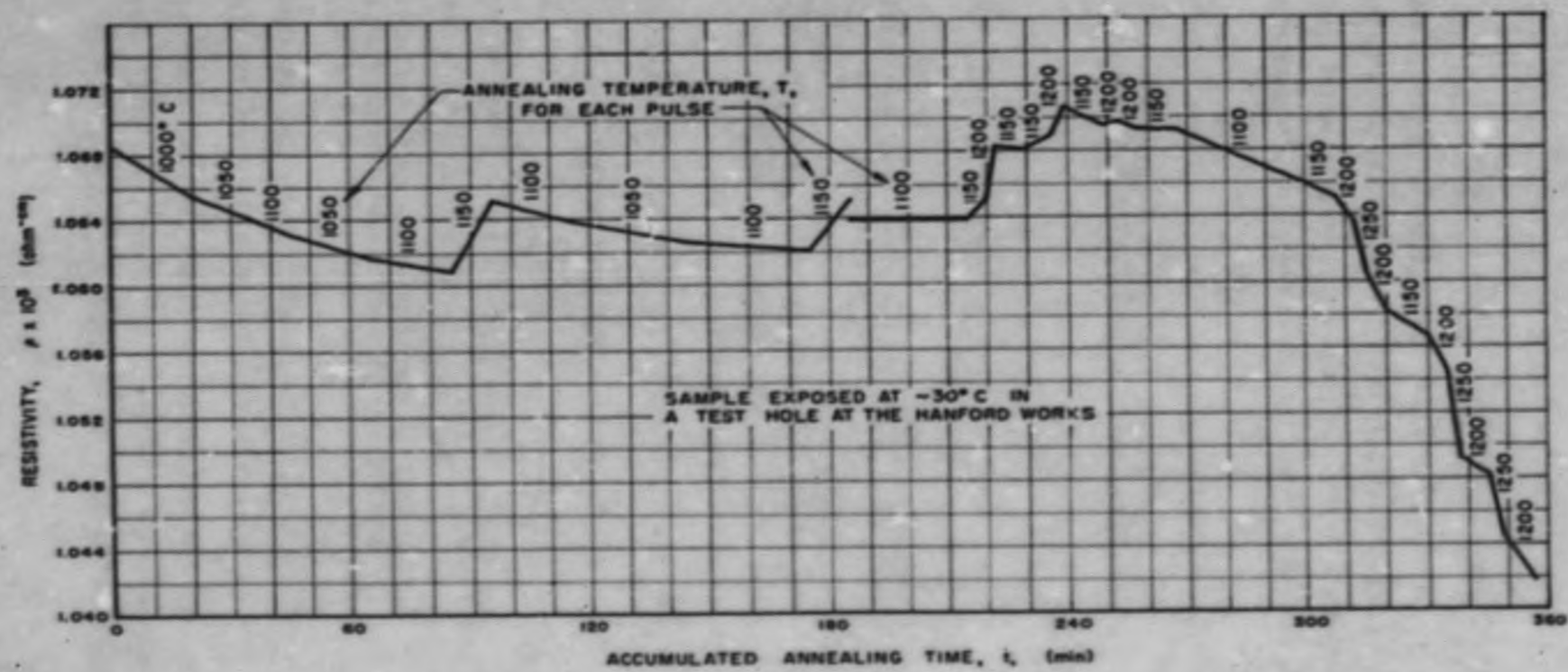


Fig. 21. Electrical Resistivity at 40°C vs Time of Various Successive Annealing Temperatures

1246 023

E. Asymptotic Aging Experiments (Robert L. Carter)

A series of experiments have been carried on in which small specimens of irradiated graphite have been partially annealed by plunging them into a constant-temperature oven. The temperature behavior of the specimen, while in the oven, is used to deduce the stored energy release rate as a function of time:

$$-\frac{dL}{dt} = C_o \left(\frac{\tau(T)}{\tau_o} \right) \left[\frac{dT}{dt} + \frac{1}{\tau(T)} (T - T_o) \right]$$

where

$\tau(T) = \frac{m C(T)}{K}$ is the instantaneous characteristic time for thermal relaxation;

$\tau_o = \frac{m C_o}{K}$ is the characteristic time for thermal relaxation near asymptotic temperature;

T is the specimen temperature;

$\frac{dT}{dt}$ is the rate of rise of specimen temperature;

T_o is the oven temperature (constant);

m is the mass of the specimen;

$C(T)$ is the specimen specific heat at temperature;

C_o is the specimen specific heat at temperature T_o ;

K is the oven-specimen heat transfer coefficient (rate of heat transfer per unit temperature difference).

The values of $\tau(T)$ and τ_o are determined from the time-temperature behavior during a second insertion of the specimen after the annealing is near completion.

If adequately low oven temperatures are selected, stored energy release will at no time cause the specimen temperature to exceed the oven temperature by more than a few degrees, and the annealing procedure may be regarded as

quasi-isothermal. Figure 22 illustrates the time-temperature behavior of a specimen of 12.5 mwd/ct Hanford cold test hold irradiated graphite during asymptotic aging at 183° C. The rate of energy release computed from the data is also shown.

It is observed that the method permits measurement of energy release rates at least an order of magnitude lower than those measurable by methods previously used. The absence of the intermittent quenchings which have been used in previous aging experiments allows the maintenance of a simple temperature history during the aging procedure. The sensitivity of the measurement and the simplicity of the temperature history permits a separation of simultaneously occurring annealing processes.

It is assumed that the rate of energy release is linearly related to the rates of annealing (or transformation) of defects of all types; i. e. .

$$-\frac{dL}{dt} = \sum_i \nu_i \left(-\frac{dn_i}{dt}\right)$$

It is further assumed that each of the annealing processes is independent of the others and is of the type,

$$-\frac{dn_i}{dt} = \nu_i n_i^{\gamma_i} \exp(-A_i/kT)$$

ν_i being the rate constant,
 γ_i the reaction order, and
 A_i the activation energy of the i th process.

Then

$$-\frac{dL}{dt} = \sum_i \nu_i u_i^{(1-\gamma_i)} L_i^{\gamma_i} \exp(-A_i/kT)$$

where we define $L_i = u_i n_i$.

▲

The key to the procedure is the high sensitivity, which permits identification of the most persistent process. The most persistent of a set of competing processes can be shown to be the one with the highest value of the order constant, γ . For processes of identical order, the one with the smallest value of the product $\nu u^{(1-\gamma)} \exp(-A/kT)$ will be observed to persist longest. In the latter case, processes inseparable at one aging temperature will become separable at another. The persistent process may be tentatively identified without accurate knowledge of the value of the associated activation energy. From the previous equation it is seen that, for process "a",

$$\begin{aligned} -\frac{dL}{dt} \Big|_a &= \nu_a u_a^{(1-\gamma_a)} L_a^{\gamma_a} \exp(-A_a/kT) \\ &= \nu_a u_a^{(1-\gamma_a)} L_a^{\gamma_a} \exp(-A_a/kT_0) \exp \left[\frac{A_a(T - T_0)}{kT_0^2} \right]. \end{aligned}$$

A normalized rate function $f'(n_a)$, corresponding to the annealing rate which would be experienced at T_0 , can be computed, giving

$$\begin{aligned} f'(n_a) &= \left(-\frac{dn}{dt} \right)_a \exp \left[-\frac{A_a(T - T_0)}{kT_0^2} \right] \\ u_a f'(n_a) &= \left(-\frac{dL}{dt} \right)_a \exp \left[-\frac{A_a(T - T_0)}{kT_0^2} \right] = \nu_a u_a^{(1-\gamma_a)} L_a^{\gamma_a} \exp(-A_a/kT_0) \\ \log u_a f'(n_a) &= \gamma_a \log L_a + \log \left[\nu_a u_a^{(1-\gamma_a)} \exp(-A_a/kT_0) \right] \end{aligned}$$

A plot of $\log u_a f'(n_a)$ against $\log L_a$ will yield γ_a . However, L_a can be obtained only within a constant by integration of $-\frac{dL}{dt} \Big|_a$.

$$\int_0^t \left(-\frac{dL}{dt} \right)_a dt = L_{0a} - L_a(t)$$



A determination of L_{0a} rests upon an estimate of the residue of the persistent-process energy which has still not appeared when the aging is terminated. A first approximation to its value for the data of Fig. 22 was made, and the curve shown in Fig. 23 was plotted. A unique refinement of L_0 was found which yielded a linear relationship between $\log u_a f'(n)_a$ and $\log L_a$ with a slope giving $\gamma_a = 3$ for the persistent process. A 20 per cent error in the estimated value of the activation energy results in no significant change in curve shape for temperature deviations of the order of one degree centigrade or less. The sensitivity of the experiments permits the bulk of the data to be obtained within this range. The value of the product, $\nu_a u_a^{(1-\gamma_a)} \exp(-A_a/kT)$, can be determined by comparison of corresponding values of $-\frac{dL}{dt}_a$ and L_a .

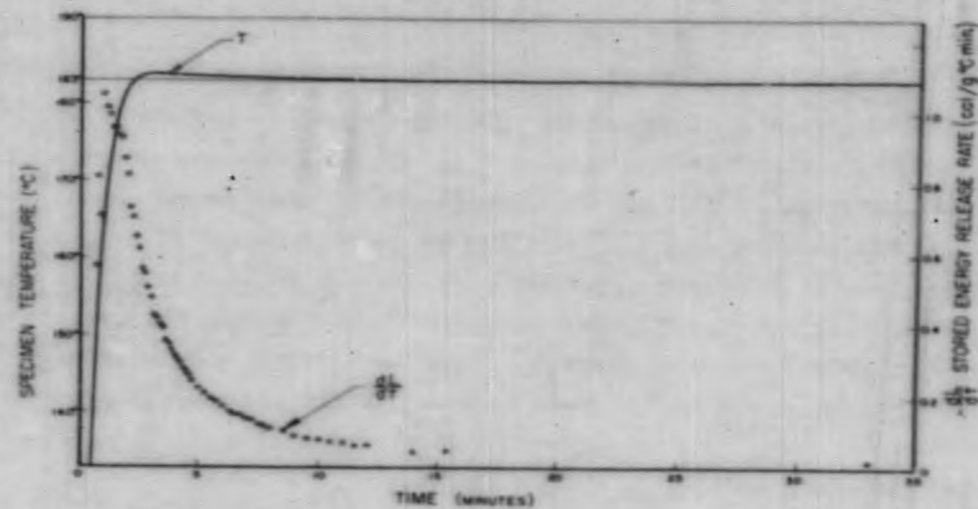
Recognition of the identity of the persistent process permits refinement of the activation energy assigned to it by comparison of values of $\nu_u^{(1-\gamma)} \exp(-A/kT)$ for annealing of identical specimens at different temperatures. The complete description of the process thus obtained can be used to integrate the process back to the beginning of the experiment, and thus obtain the residual process energy and energy release rates:

$$-\left(\frac{dL}{dt}\right)_r = \left(-\frac{dL}{dt}\right) - \left(-\frac{dL}{dt}\right)_a$$

$$L_r = L - L_a$$

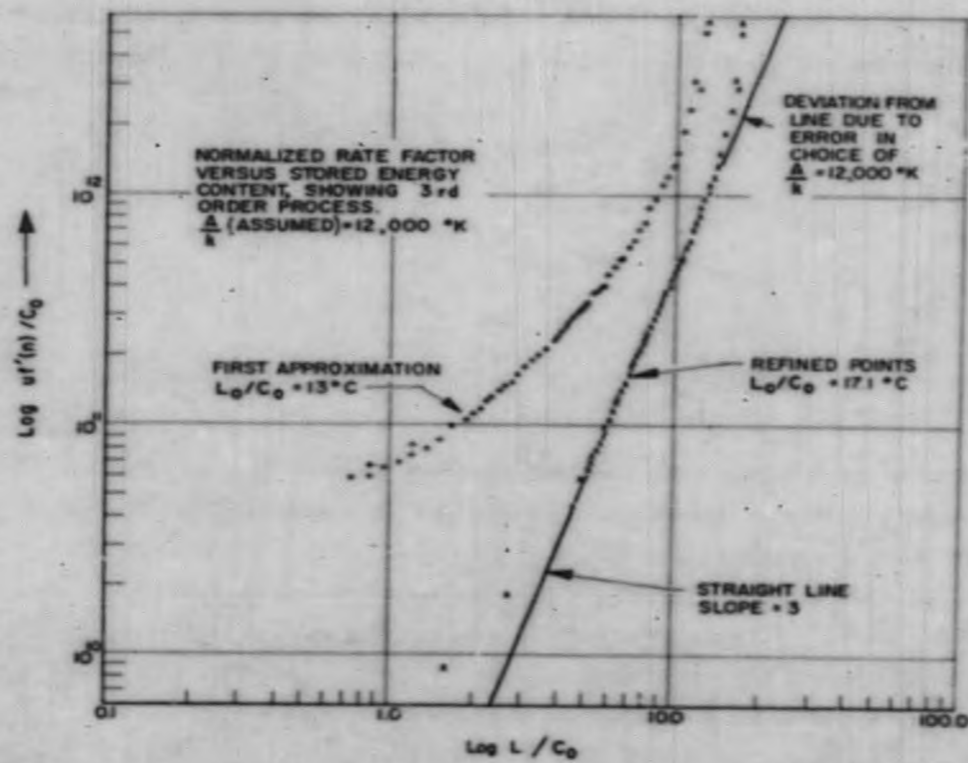
The analytical process is repeated to separate the second most persistent process, and so on.

Results obtained to date have established the existence of a persistent third order process and two first order processes for the annealing of stored energy from graphite in the range from 170 to 200° C. The histories and aging conditions for the samples measured thus far are given in Table I. Tentative evaluations of $L_0 \nu_u^{(1-\gamma)} \exp(-A/kT)$ and $\frac{A}{k}$ are given in Table II. The contents of Table II are to be regarded as provisional and will probably be subject to extensive adjustment as a result of work now underway.



SECRET - 543-2540

Fig. 22. Stored Energy Release from Irradiated Graphite Annealed in an Oven at 183° C



SECRET - 543-3140

Fig. 23. Thermal Annealing of 12.5 md/ct Irradiated Graphite

TABLE I
AGING CONDITIONS

Annual Run Number Date	Sample Number & Graphite Type	Sample Irradiation (md/ct)	Irradiation Temperature	Completion Date of Irradiation	Annual Period To* Min.	Annual Temperature To °C	Temperature Range Over Which Calculated	
							Min. °C	Max. °C
6/26/53	87-202 KC	12.5	~ 30	7-49	0.48	202.9	175.8	203.9
7/17/53	87-202 KC	12.5	~ 30	7-49	0.53	183	141	183.8
7/21/53	87-216 KC	48	~ 30	8-49	0.66	183.5	124	188.5
7/27/53	87-215 KC	146	~ 30	10-49	0.55	170	130	180
7/28/53	87-207 KC	460	~ 30	7-50 (?)	0.44	170	110	191
7/30/53	293 KC	1534	30 (?)	48 (?)	0.54	170	150	173
8/21/53	HE-53 AWG	92	50	7-53	0.69	171	100	188
8/24/53	C-488A AWG	7.7†	35	5-52	0.155	170	118.5	170.5
8/25/53 I	HE-54 AWG	41	50	2-53	0.69**	171	96	176
8/25/53 II	HE-51 AWG	126	50	9-52	0.69**	171	115	192.6

* Variations in anneal period are assignable to large deviations from nominal specimen dimensions.
 † α irradiation from cyclotron measured in $\mu\text{a}\cdot\text{hr}/\text{cm}^2$.
 ** Estimated values.

1246 029
31

TABLE II
PROVISIONAL RESULTS

Annual Run Number Date	Persistent Process			Residual Process "A"			Residual Process "B"		
	$\frac{A}{k}$ °K	L_0 Cal/gm	$\frac{A}{a^2} e^{-A/kT}$ (gm/cal) ² Min ⁻¹	$\frac{A}{k}$ °K	L_0 Cal/gm	$\frac{A}{k} e^{-A/kT}$ Min ⁻¹	$\frac{A}{k}$ °K	L_0 Cal/gm	$\frac{A}{k} e^{-A/kT}$ Min ⁻¹
6/26/53	9,400	4.75	8.4×10^{-2}						
7/17/53	13,300 † 8,100	4.67	2.5×10^{-2} $1.05 \times 10^{-2} \dagger\dagger$						
7/21/53	9,800	14.3	3.7×10^{-3} $1.5 \times 10^{-3} \dagger\dagger$						
7/27/53	10,000 **	23.1	1.8×10^{-3}	13,200	7.88	0.56	(Residual processes inseparable)		
7/28/53	10,000 **	29.2	5.8×10^{-5}	13,200 **	5.52	0.56	12,170	11.0	2.88
7/30/53	10,000 **	15.5	2.7×10^{-4}	10,000	3.0	0.8	(Residual processes inseparable)		
8/21/53	10,000 **	15.9	1.6×10^{-4}	13,200 **	2.45	0.25	9,800	12.06	2.3
8/24/53				13,200 **	1.87	0.31	22,000	0.87	1.81
8/25/53 I	10,000 **	11.2	5.2×10^{-4}	13,200 **	1.52	0.44	10,700	5.5	1.64
8/25/53 II	10,000 **	19.7	7.7×10^{-5}	13,200 **	2.85	0.34	8,640	13.7	5.75

† Value derived by comparing rate parameters for the two runs.
 $\frac{A(\Delta T)}{kT^2}$

†† Values normalized to 170° C by multiplying by e
** Estimated values.

M40 030



II. METALS



A. Effects of Impurities on the Recovery of Electrical Resistivity in Cold-Worked Copper (J. A. Brinkman, R. D. Burch)

Three annealed copper wires were reduced in diameter from 0.0100 inch to 0.0031 inch by drawing through a series of dies at room temperature. One specimen contained 0.1 atomic per cent silver as an impurity, another contained 0.1 atomic per cent zinc, while the third was 99.999 per cent pure copper. Following the cold work, each was annealed by heating in a wax bath at a uniform rate of 2.5° C/min. At 5° C intervals, each specimen was rapidly cooled and its residual resistivity (electrical resistivity at liquid helium temperature) measured. The tempering curves are shown in Fig. 24.

The resistivity change of the Cu + Ag specimen is about 50 per cent greater than that of the pure Cu for the same amount of cold work, indicating that the presence of the silver atoms enhances the production of lattice defects by the cold work. The resistivity change of the Cu + Zn, on the other hand, is only about 10 per cent greater than that of the pure Cu, indicating that the enhancement of the production of lattice defects by zinc atoms is much smaller than by silver atoms during cold work.

An examination of the shape of the tempering curves shows that an appreciable portion of the extra resistivity change observed in Cu + Ag recovers between 100 and 150° C. The tempering curves for Cu + Zn and pure Cu are identical up to 150° C, while the resistivity change in Cu + Ag to this temperature is over twice as large, the excess being obvious as a rather sharp drop, commencing at about 100° C and ending at 150° C. It has been argued earlier¹² that this is the temperature range in which excess vacancies migrate in copper, and that the activation energy for their migration is 1.19 ev. Therefore, it is believed that the present observations offer evidence that the production of vacancies in copper during cold work is enhanced by the presence of larger atoms, such as silver, but is essentially unaffected by the presence of zinc atoms, which are nearly the same size as the copper atoms.

The main part of the residual resistivity induced in Cu + Ag by cold work does not recover until about 350° C, for this particular heating rate, while in



pure Cu it recovers at about 210° C. This agrees with the general observation that the recovery temperature is increased by the presence of impurity atoms. In the Cu + Zn, however, the opposite effect is observed; the zinc lowers the recovery temperature by about 20° C. This effect cannot be explained at present.

The tempering curve for the specimen containing silver shows a considerable amount of fine structure. Besides the 100 to 150° C state, which has been ascribed to vacancy migration, and the final recovery state from 350 to 400° C, there appears to exist another state between about 220 and 270° C, as there is a pronounced dip in the tempering curve here. This state has not been studied in detail, and it is not known whether a unique activation energy can be assigned to it. Let us assume, for the moment, that a definite activation energy is associated with this state and that the activation energies for the different states are proportional to the absolute temperature at which the recovery is observed in such a tempering curve. Then, as the activation energy for the vacancy migration state is 1.19 ev, the activation energy for this state can be estimated as about 1.55 ev. Because this is close to the activation energy for diffusion of silver into copper, it is suggested that this recovery state may result in some manner from migration of the silver atoms by the normal diffusion mechanism.

Further studies are being made in an attempt to determine the activation energies associated with the various recovery states.

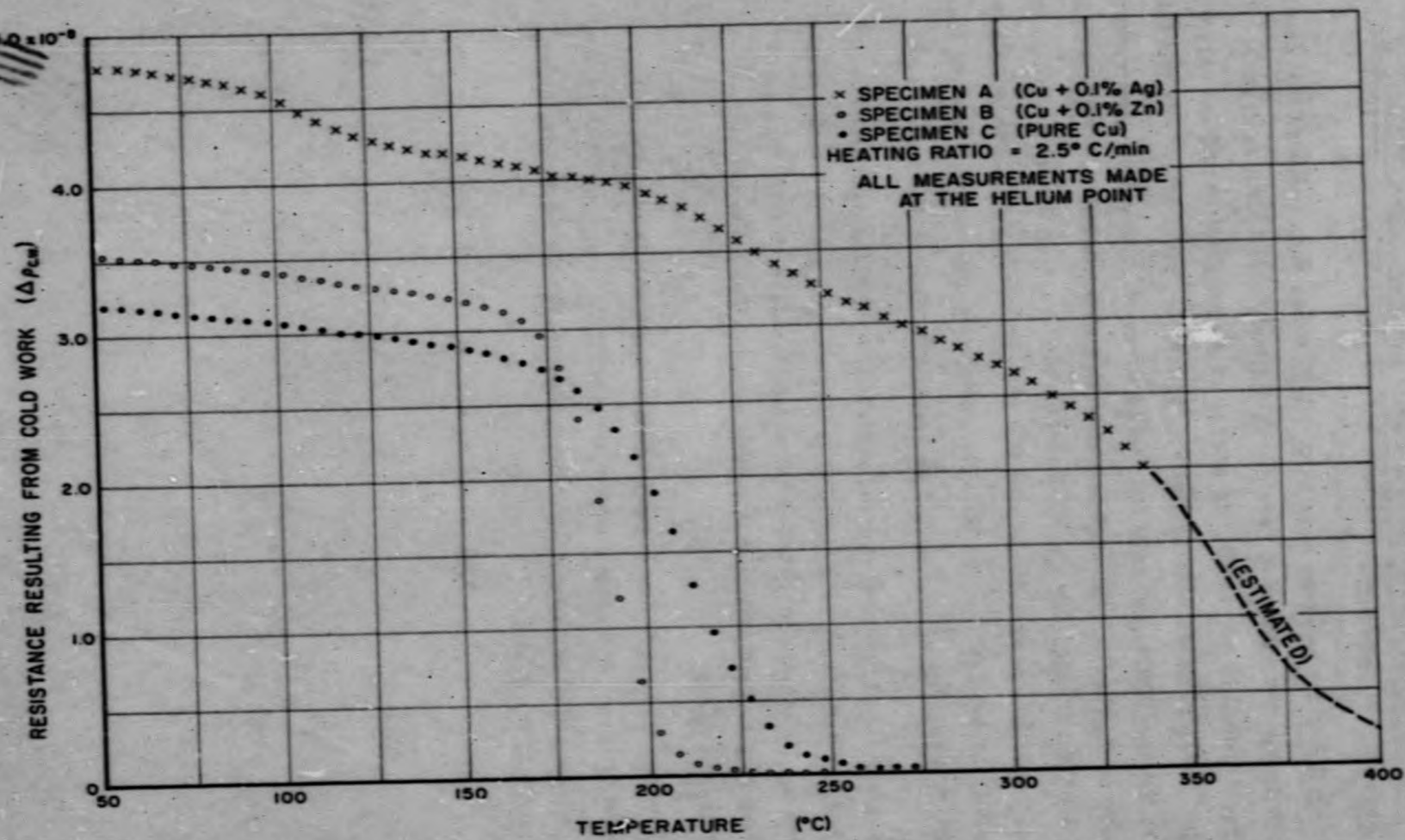


Fig. 24. Tempering Curves Showing Recovery of Residual Electrical Resistivity of Cold-Worked Pure Copper and Copper Containing Silver and Zinc Impurities

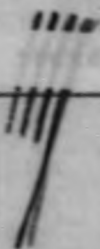

1246 033 35



B. Measurements of Thermoelectric Power and Electrical Resistivity of Copper (G. W. Rodeback)

In much of the work we have been doing, it has been assumed that damage does not change the number of carriers in a simple metal such as copper. If this should indeed be so, the Fermi energy of the material should not vary with damage. Measurements have been made for the electrical resistivity and the relative thermoelectric power of four small wires of commercial-purity copper with varying degrees of cold work and annealing in the temperature range from 140 to 300° K. By applying the Sommerfeld free-electron theory of conduction and thermoelectric power, it is found that the calculated Fermi energy is constant within experimental error over the complete range of cold work and temperature of measurement. This result holds true whether one assumes the damage gives rise to point scattering centers (such as impurity atoms might be), or area scattering (such as grain boundaries or slip bands might give rise to). Photomicrographs of the grain structure indicate that the scattering may be primarily due to boundaries, but the matter is not yet completely resolved.

A copper sample is now being irradiated with alpha particles in the Berkeley Cyclotron, and copper specimens having 0.3 and 1.0 atomic per cent of tin have been prepared in an attempt to resolve the uncertainties as to the nature of the defect.




C. Elastic Constants and Internal Friction (H. Dieckamp)

Work on elastic constants and internal friction has continued in the direction of obtaining complete annealing curves for cold-worked copper over the annealing temperature range from -196° to $+300^{\circ}$ C. The complete annealing study involves shear-modulus and internal-friction measurements at -196° C for about six different frequencies in the range from 0.3 to 0.9 cycles per second after each anneal. The temperature of anneal is increased 25° C each time. All measurements are made on polycrystalline wires in torsion. The working is done by twisting.

Recent measurements of the shear modulus and the internal friction for various degrees of cold work at -196° C indicate that practically all of the observed modulus decrease of about 10 per cent occurs upon straining to a surface shear of 0.1. Further straining causes only a small additional change. The internal friction rises rapidly for low strains and reaches a maximum at a surface shear of about 0.4. A similar behavior has been observed for single crystals of copper by Weertman and Koehler.¹³

As the cold-work data become more complete, it is interesting to speculate on the possible mechanisms associated with the changes. The most promising view seems to be to ascribe the modulus reduction and the internal friction increase to the motion of dislocations. The recovery of the modulus and the internal friction suggests, in addition to the annihilation of dislocations or their agglomeration to grain boundaries, the possibility of major changes occurring as a result of the interaction of dislocations with interstitials and vacancies.

Measurements on radiation-damaged specimens, in which the primary effects should be due to interstitials and vacancies, should greatly illuminate the interpretation. A cyclotron target box has been completed, and an irradiation has been scheduled for the first week in November at the Crocker Laboratory in Berkeley.




D. Radiation Effects in Metastable Alloys (J. M. Denney)

The investigation of the effect of radiation on metastable alloys of iron in copper, as originally planned, has been completed. A detailed description of the results of this investigation is presented in forthcoming reports, and will not be discussed in detail here.

The comparison of the observed precipitate transformation rate due to high energy electron bombardment has been completed. The results indicate satisfactory agreement between the theory and experiment. In the experiment the coherent face-centered cubic iron precipitate in an alloy of 2.4 weight per cent iron in copper was observed to transform during irradiation to a non-coherent structure which was ferromagnetic. The coherent face-centered cubic precipitate is paramagnetic, thus enabling the determination of the amount of transformed precipitate by the measurement of the saturation magnetization. In this way it was found that approximately 200 iron atoms are transformed for each iron atom displaced from its lattice site as a result of elastic collision by the incident electron. Agreement between theory and experiment could not be obtained on the assumption that precipitate transformation was due to ionization along the path of the electron in the alloy. These results support the hypothesis that the radiation-induced change is due to atomic displacement produced as a result of elastic collisions and is not due to ionization.

Analysis of data obtained from irradiating metastable alloys of iron in copper with cyclotron particles has been nearly completed. Surprisingly, the heavier cyclotron particles (proton and alpha particles) are not as effective in transforming the metastable precipitate as the high energy electrons mentioned above. The basis of comparison here is in the number of atomic displacements expected as a result of irradiation by the respective particles. This apparent anomaly may be interpreted in the following manner. Analysis of the rate of producing displacements along the path of the primary recoil atoms has led Brinkman¹⁴ to postulate a melted region, denoted as a "displacement spike, at the end of the path of the primary knock-on. Evidently the effect of such a melted region will be opposite to the effect of single displacements. The melted region will serve to mix, by melting, the iron precipitate the copper matrix. The alloy after solidification of the displacement spike will be returned to a supersaturated solid solution in the melted region. The rate of formation of



regions of transformed precipitate will thus be reduced by displacement spikes by dissolving previously transformed regions and by reducing the amount of precipitate available for transformation. Preliminary calculations based upon the above mechanism and Brinkman's postulated displacement spike using the experimental data from the cyclotron irradiations indicate that the volume of the displacement spikes in copper is of the order of 2×10^4 atoms. This shows remarkable agreement with the value of 10^4 atoms/spike predicted by Brinkman. A more careful treatment of this problem will soon be published.

In an effort to obtain more direct evidence for the effect of the displacement spike in this alloy, a somewhat different experiment was performed. In previous experiments the metastable precipitate was transformed to the ferromagnetic stable form by irradiation. The reverse process was found to be impossible, except by thermal re-solution and precipitation. Single atomic displacements cannot achieve the reverse; however, a displacement spike would be capable of producing re-solution in isolated regions of the alloy. Thus a direct measurement of displacement spikes was provided by irradiating an alloy with the stable form of the precipitate fully developed. A decrease in the amount of the ferromagnetic precipitate could only be due to displacement spikes. Such a decrease was observed* after bombardment with protons in the cyclotron. Preliminary estimates of beam intensity and distribution indicate agreement with the previously obtained value of 2×10^4 atoms/spike. It is felt that this result offers direct experimental evidence for the existence of displacement spikes.

*These observations were obtained from saturation magnetization measurements described in detail in NAA-SR-270.¹⁵



III. INSULATORS

A. Mechanical Effects of Ionizing Radiation in Insulators (D. Westervelt)

An effort has been made to interpret the hardness changes in irradiated alkali halide crystals, which were described in the last quarterly report,¹⁶ in terms of specific radiation-induced lattice defects. In particular, a correlation of the radiation effects with earlier reports of the effects of divalent impurity ions on the critical shear stress and the tensile strength has led to assignment of the largest part of the radiation-induced hardness to positive ion vacancies. This explanation of the effect of irradiation is of particular value in the interpretation of low energy bombardments, such as those in which X-rays are used. In such irradiations the production of lattice damage by direct atomic displacement is inherently impossible. It can be demonstrated, however, that the formation of vacancies by a mechanism involving their dissociation from edge dislocations occurs during any ionizing irradiation.

The results of hardness measurements which were made on synthetic rock salt crystals containing calcium and cadmium as impurities appear to support the theory of vacancy-induced hardness. A final conclusion based on these results will not be possible until the impure crystals grown during this quarter have been chemically analyzed for their impurity content, but preliminary results show a large hardness increase in a crystal containing calcium as an impurity, in which the impurity-induced positive vacancies are largely free and atomically dispersed in the crystal lattice, and a much smaller increase in a crystal containing cadmium. In the latter case, it is known that the vacancies are largely associated with the impurity ions in the form of divalent ion-vacancy complexes. These results, together with the interpretation of radiation-induced hardness changes, will be described in a report to be issued shortly. In this report experiments are described which will provide a crucial test of the theory of vacancy-induced hardness in solids, thus far not subjected to direct experimental verification. The results which are described emphasize the significant influence of the effects of ionization or, more exactly, of the photoelectrons and excitons freed in the lattice as a result of the ionizing radiation on a large number of physical properties of insulators which in other materials would be expected to be unaffected by radiation except when atomic displacements are produced.

OK in Ord
for APL/JM

B. Optical Effects in Alkali Halides (D. Westervelt, V. Martin)

Investigation of the optical effects of radiation on the alkali halides has continued, the effort during this quarter being directed chiefly toward clarification of a number of questions raised by the earlier measurements and toward improving the experimental techniques in such a way as to place the results on a firmer quantitative basis. Several previously unexplained effects have been traced to the influence of oxygen on the colored crystals during annealing, and all thermal anneals at present are being carried out in evacuated pyrex tubes. A series of experiments is in progress in which the effects of annealing in the dark are compared with results obtained when the crystals are exposed to visible light during annealing. It has already been reported¹⁶ that the optical transformations (together with the associated hardness changes) are greatly accelerated by visible illumination, and the question arises whether the end result of annealing is the same in both cases. It was also reported¹⁶ that no difference had been observed in this end result. Further clarification of the problem results from the curves in Figs. 25, 26, and 27 which are the absorption spectra of two fragments of a single additively colored crystal of KCl. One fragment was annealed at about 150° C in the dark for a period of 7-1/2 days (Fig. 25). The other was annealed at the same temperature in the daylight, first for 5 minutes (Fig. 26) and then for the same total period as the other fragment (Fig. 27). Spectra both at room temperature and at liquid nitrogen temperature are shown. Examination of the graphs shows that the 5 minute anneal in daylight resulted in a much broader absorption band, the peak of which was at a somewhat longer wave length and was less temperature dependent than the peaks of the bands present in both crystals after the longer anneals. The latter, on the other hand, are more nearly equal in breadth, and precisely the same in peak wave length, the maximum in absorption in both cases occurring at a wave length of 700 millimicrons. (The crystals were also measured after 3 and 28 days, and the peak locations were the same, 700 m μ .) In addition, the peaks at 700 m μ in both crystals exhibit a property which, to the writer's knowledge, has never before been observed in colored alkali halides: when the crystal is cooled to liquid nitrogen temperature, the peak

of the absorption band shifts about $10\text{ m}\mu$ to longer wave lengths. The effect is small, but entirely reproducible, and it has been observed in a number of crystals after they were annealed until the peak wave length no longer changed upon further annealing. A shift of the peak wave length in this direction upon cooling may be explainable in terms of the colloidal particle theory of the $700\text{ m}\mu$ absorption band, if the particles are assumed to contract faster than the surrounding crystal lattice, thereby relieving the local strain in the lattice and effectively increasing its index of refraction. However, the location of this absorption band depends on the optical properties of the metal particles as well as those of the crystal, and thus the shift may be due to the low temperature characteristics of these metallic properties. A detailed interpretation must await the results of experiments now in progress.

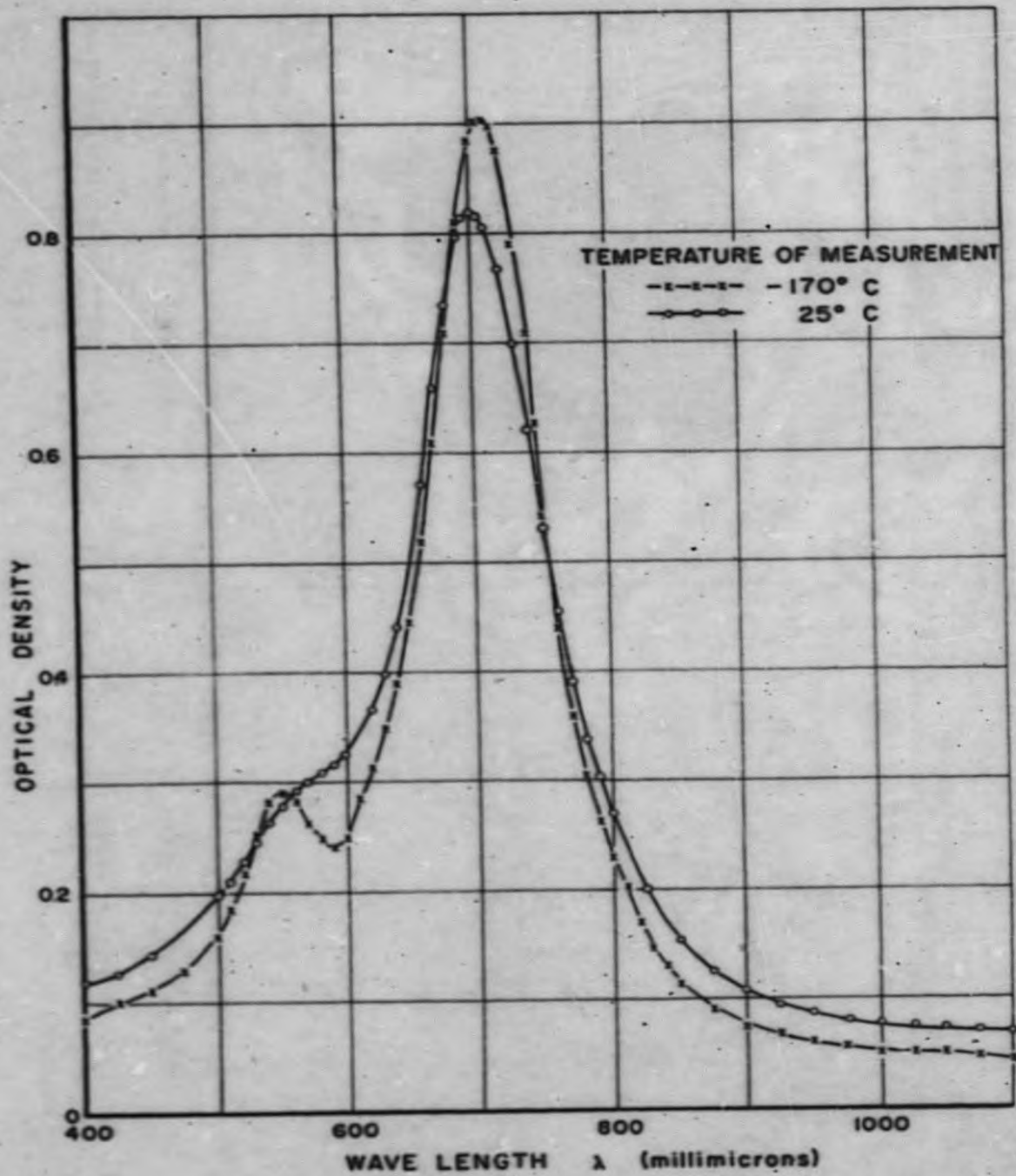


Fig. 25. Optical Absorption of Additively Colored KCl after 180 hours at 150°C (Annealed in Dark)

OK Ba Ord
44 BY APL/JMU

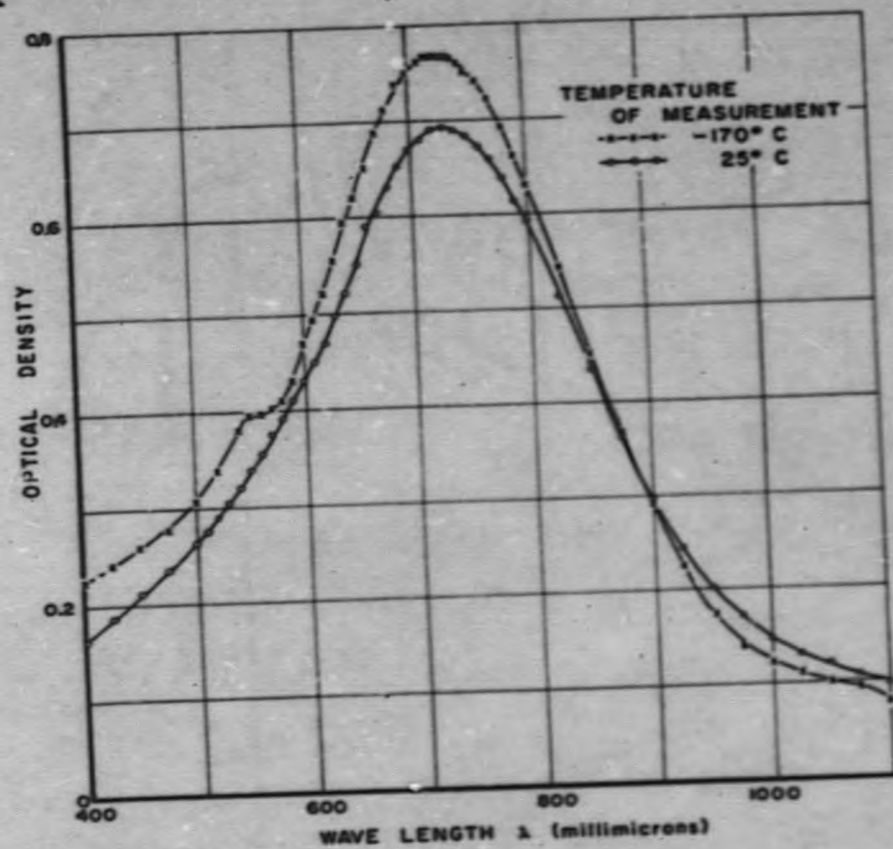


Fig. 26. Optical Absorption of Additively Colored KCl after 50 minutes at 150° C (Annealed in Daylight)

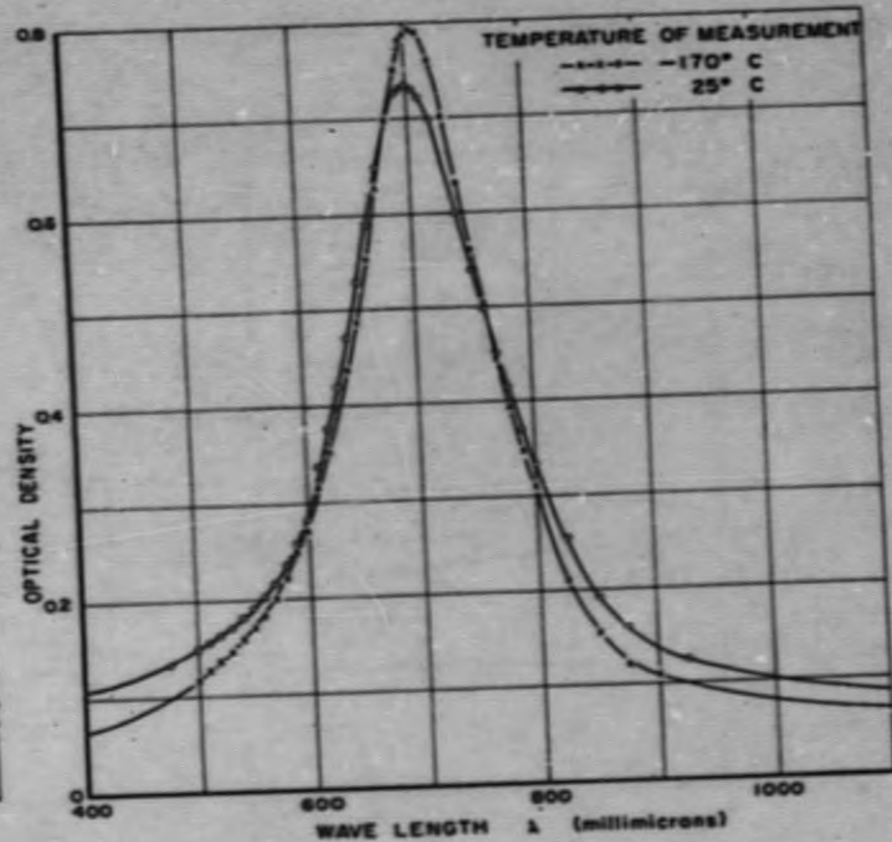


Fig. 27. Optical Absorption of Additively Colored KCl after 180 hours at 150° C (Annealed in Daylight)

11276 042



IV. CYCLOTRON OPERATION AND DEVELOPMENT

A. Operation (A. Andrew)

During this quarter, the 60-inch cyclotron at Crocker Laboratory was used a total of 65 hours for radiation damage studies. Irradiations were made in order to determine the effect of radiation on the following properties:


1. Thermoelectric power of graphite
2. Ordering and disordering of Cu_3Au
3. Excitation function of alphas on copper and 302 stainless steel
4. Magnetic state of a solution of Fe in Cu
5. Hardness of steel (for NRDL)

B. Radiation Effects on Thermoelectric Power of Iron (A. Andrew, C. R. Davidson)

The apparatus has been redesigned by incorporating individual heater controls in order to provide better control over the absolute temperature and the temperature difference between the hot and cold junctions. A range of temperature differences between the junctions of from 5 to 25° C is now available. Bubbling helium through the liquid nitrogen in the bottom of the dewar has increased the heat capacity of the region around the target, thus speeding up the thermal response of the system. This redesign permits dynamic measurements to be made with less error due to thermal lags.

The spurious emf's at the copper-iron junctions have been reduced to less than 0.5 per cent by placing the individual junctions in small thin walled glass tubes which are suspended in a multilayer radiation shield of aluminum foil. The whole assembly is then thermally insulated by means of an empty dewar. The air-annealed iron leads have also been replaced with vacuum-annealed iron leads specifically chosen by testing for thermoelectric homogeneity.

A calibration run was made using a piece of constantan wire instead of the irradiated iron wire to determine geometric temperature errors. An average uncertainty of 2 per cent was found in the temperature difference in the range from +25 to -195.6° C. The uncertainty in the emf's is estimated to be about 4 per cent over the same temperature range, which corresponds to an average



uncertainty of about 5 per cent in the thermoelectric power. The remaining spurious emf's are due to thermoelectric inhomogeneities presumably caused by residual cold work, spot welding, and compositional variations in the lead wire. We were unable to detect any spurious emf's due to oxide film formation. The data are given in Fig. 28. One value of the thermoelectric power from previous work¹⁷ is included for comparison.

C. Rotating Target Holder (B. T. Harwick)

A target holder has been designed and built to irradiate wire targets uniformly over a length of about 36 inches at a temperature of -196°C . The holder consists of a rotating, helically grooved lavite spool mounted on a horizontal spindle. Stainless steel ball bearings have been used throughout. The design represents the best compromise between maximum use of the 1-1/2 inch by 1/4 inch beam and minimum cold work of the sample due to mounting.

D. Mass Transfer of Radioactivity (L. S. Glasgow)

An approximate excitation curve for 40-Mev alpha particles incident on 302 stainless steel has been made using the stacked foil technique. The curve indicates that below 10 Mev the alpha induced activity after 60 days is less than 50 d/sec/ $\mu\text{ab}/\text{gm}$ of stainless steel. The activity is due to 70-day Co^{58} [$\text{Mn}(\alpha, n)\text{Co}^{58}$]. No other long lived isotopes are indicated. The total alpha induced activity for a cyclotron experiment of 48 hours will be of the order of 10^4 d/sec/gram, which may be neglected when compared to the initial source strength of 10^8 d/sec/gram.

E. Physical Length Change of Graphite (J. H. Pepper)

The apparatus which was used to measure the physical length change of damaged graphite as a function of thermal annealing was modified in accordance with previous recommendations.¹⁸ The equipment consists of a differential transformer-extensometer unit capable of measuring length changes as small as 5 micro-inches. Length changes are recorded on an L and N 16 channel Speedo-max.

Two separate runs were made on damaged graphite samples (0.75 inch by 0.1 inch by 0.02 inch) with a probable damage history of 460 mwd at 30°C . Their exact history, however, is not known. The first sample showed a physical length contraction of 0.16 per cent after being subjected to a thermal



pulse of 280° C for 2.2 hours. Repeated thermal pulsing at higher temperatures (up to 365° C) for a period of 4 hours increased the total contraction to 0.18 per cent.

The second sample underwent larger changes in physical length. The initial thermal pulse of approximately 120° C for 40 seconds produced a physical length contraction of 0.3 per cent. Further thermal pulsing to temperatures as high as 500° C for 3.4 hours resulted in a total contraction of 0.8 per cent. The rapid rate of change of length in the specimen during the first few minutes is in agreement with other studies of the thermal annealing of damaged graphite, particularly the report of Bacon.¹⁹

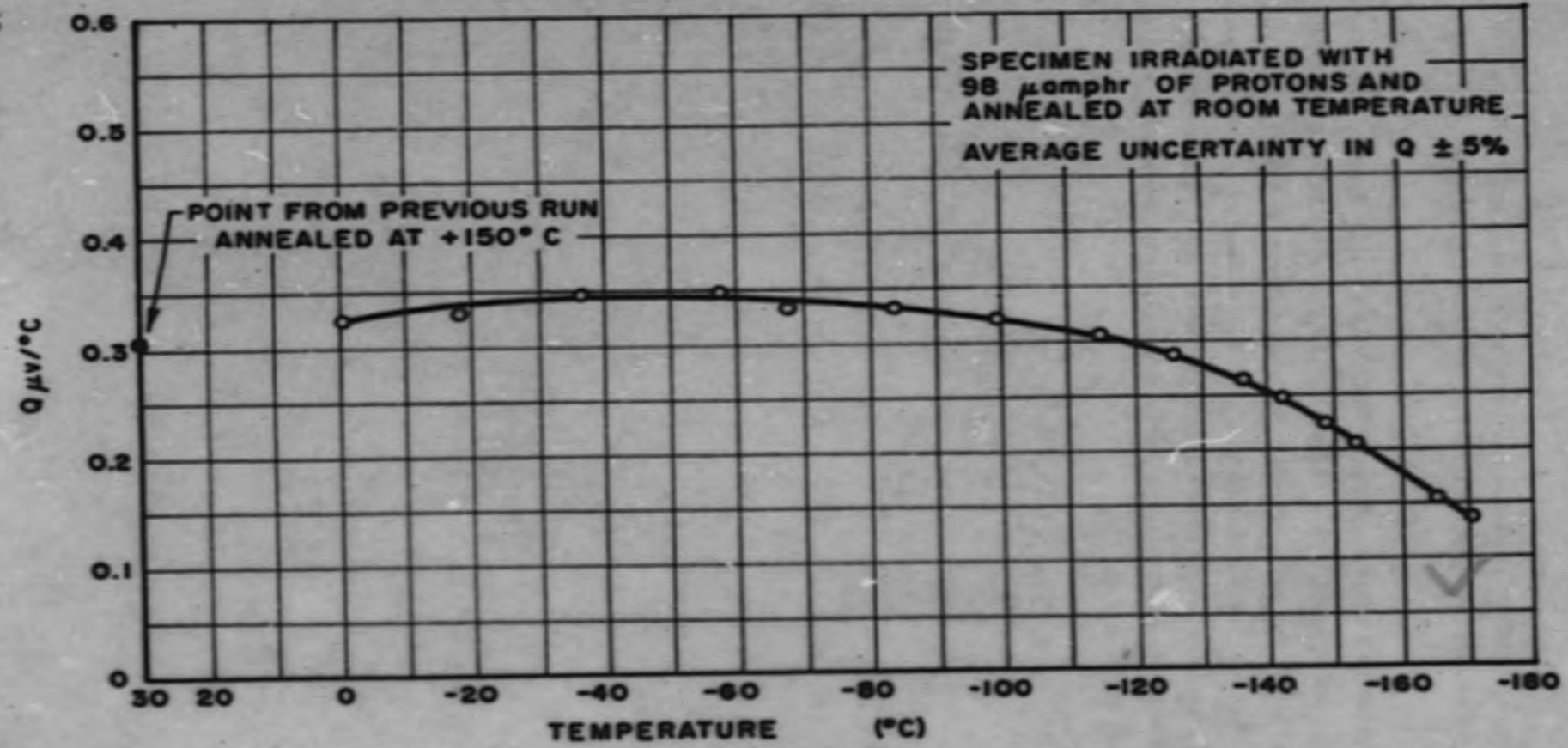



Fig. 28. Thermoelectric Power vs Temperature for Iron-Irradiated Iron

1256 046



V. REACTOR IRRADIATIONS

A. Capsule Exposures (D. J. Klein)

The assembly of the capsules containing graphite samples for irradiation in MTR lattice positions is again underway after some delay caused by a heavy shop load. The capsules will probably be shipped to Idaho before November 1, 1953.


B. In-Pile and Related Experiments (D. J. Klein, R. E. Durand, M. J. Laubenstein)

The post-irradiation analysis of the uranium-impregnated graphite samples exposed at elevated temperatures in the MTR has been completed, and a topical report covering the work will soon be issued.

Assembly of the first experimental plug for the determination of changes in the thermal conductivity of graphite in the temperature range from 300 to 700° C is near completion. It is expected that the plug will be shipped to the MTR site sometime during the month of October.

Construction of the equipment to determine if the presence of γ -rays will enhance the thermal annealing of damaged graphite is nearly complete.*

*This experiment is being carried out as a cooperative project with the Phillips Petroleum Company.



REFERENCES

1. Smith, A. W., "The Thermal and Electrical Conductivities of a Graphitized Lampblack as a Function of Temperature and Neutron Irradiation," pages 10-13 of "Solid State and Irradiation Physics Quarterly Progress Report, April-June, 1953," NAA-SR-268, December 1, 1953.
2. Rasor, N. S., and A. W. Smith, "Low Temperature Thermal and Electrical Conductivities of Normal and Neutron Irradiated Graphite," NAA-SR-862, to be published.
3. Krumhansl, J., (private communication).
4. McClelland, J. D., "The Paramagnetism Associated with Radiation Damage in Graphite," pages 13-15 of "Solid State and Irradiation Physics Quarterly Progress Report, April-June, 1953," NAA-SR-268, December 1, 1953.
5. Eatherly, W. P., and N. S. Rasor, "The Thermoelectric Power of Graphite: Dependence on Temperature, Type, and Neutron Irradiation," NAA-SR-196, November 21, 1952.
6. Deegan, G. E., "The Measurement of Damage as a Function of Depth in Cyclotron Irradiated Graphite," pages 15-21 of "Solid State and Irradiation Physics Quarterly Progress Report, April-June, 1953," NAA-SR-268, December 1, 1953.
7. Faris, F., "Results of Resistivity-Range Measurements on Graphite Bombarded with Charged Particles," NAA-SR-14, October 12, 1950.
8. Austerman, S. B., and R. L. Carter, "Annealing Kinetics," pages 50-66 of "Solid State and Irradiation Physics, Quarterly Progress Report, October-December, 1952," July 2, 1953.
9. Austerman, S. B., "Annealing Kinetics," pages 10-18 of "Solid State and Irradiation Physics Quarterly Progress Report, January-March, 1953," NAA-SR-251, October 8, 1953.
10. Austerman, S. B., "Annealing Kinetics," pages 21-22 of "Solid State and Irradiation Physics Quarterly Progress Report, April-June, 1953," NAA-SR-268, December 1, 1953.
11. Hock, A. S., "Changes in the Thermal and Electrical Properties of Irradiated Graphite During Pulse-Annealing," NAA-SR-119, January 24, 1952.
12. Brinkman, J. A., C. E. Dixon, and C. J. Meehan, "Interstitial and Vacancy Migration in Cu_3Au and Copper," NAA-SR-249, August 4, 1953.
13. Weertman, J., and J. S. Koehler, "Internal Friction and Young's Modulus of Cold-Worked Copper Single Crystals," *Journal of Applied Physics*, 24, 624-631, (1953).
14. Brinkman, J. A., "On the Nature of Radiation Damage in Metals," NAA-SR-198, December 22, 1952.
15. Denney, J. D., "Precipitate and Structure in a Metastable Alloy of Iron in Copper," NAA-SR-270, (to be published.)

1111



REFERENCES (Continued)

16. Westervelt, D. R., "Thermal Annealing of Radiation-Induced Hardness Changes in Alkali Halides," pages 34-42 of "Solid State and Irradiation Physics Quarterly Progress Report, April-June, 1953," NAA-SR-268, December 1, 1953.
17. Andrew, A., and C. R. Davidson, "Radiation Effects on Thermocouple Materials," pages 133-134 of "Solid State and Irradiation Physics, Quarterly Progress Report, October-December, 1952," NAA-SR-229, July 2, 1953.
18. Pepper, J. H., "Feasibility Study - Physical Length Change of Graphite," pages 44-45 of "Solid State and Irradiation Physics, Quarterly Progress Report, April-June, 1953," NAA-SR-268, December 1, 1953.
19. Bacon, G. E., "The Effect of Pile Irradiation on the Unit Cell Dimensions of Graphite," AERE-G/R-1079, December, 1952.

END

SECRET